

Mechanisms for a nutrient-conserving carbon pump in a seasonally stratified, temperate continental shelf sea

Matthew P. Humphreys^{1,2,*}, Eric P. Achterberg^{1,3}, Joanne E. Hopkins⁴, Mohammed Z. H. Chowdhury¹, Alex M. Griffiths¹, Susan E. Hartman⁵, Tom Hull^{2,6}, Angelina Smilenova¹, Juliane U. Wihsgott^{4,7}, E. Malcolm S. Woodward⁸, C. Mark Moore¹

¹ Ocean and Earth Science, National Oceanography Centre Southampton, University of Southampton, Southampton, UK

² Centre for Ocean and Atmospheric Sciences, School of Environmental Sciences, University of East Anglia, Norwich, UK

³ GEOMAR Helmholtz Centre for Ocean Research, Kiel, Germany

⁴ National Oceanography Centre, Liverpool, UK

⁵ Ocean Biogeochemistry and Ecosystems, National Oceanography Centre, Southampton, UK

⁶ Centre for Environment, Fisheries and Aquaculture Science, Lowestoft, UK

⁷ Department of Earth, Ocean and Ecological Sciences, School of Environmental Sciences, University of Liverpool, UK

⁸ Plymouth Marine Laboratory, Plymouth, UK

* Corresponding author (matthew.humphreys@uea.ac.uk)

Abstract

Continental shelf seas may have a significant role in oceanic uptake and storage of carbon dioxide (CO₂) from the atmosphere, through a ‘continental shelf pump’ mechanism. The northwest European continental shelf, in particular the Celtic Sea (50°N 8°W), was the target of extensive biogeochemical sampling from March 2014 to September 2015, as part of the UK Shelf Sea Biogeochemistry research programme (UK-SSB). Here, we use the UK-SSB carbonate chemistry and macronutrient measurements to investigate the biogeochemical seasonality in this temperate, seasonally stratified system. Following the onset of stratification, near-surface biological primary production during spring and summer removed dissolved inorganic carbon and nutrients, and a fraction of the sinking particulate organic matter was subsequently remineralised beneath the thermocline. Water column inventories of these variables throughout 1.5 seasonal cycles, corrected for air-sea CO₂ exchange and sedimentary denitrification and anammox, isolated the combined effect of net community production (NCP) and remineralisation on the inorganic macronutrient inventories. Overall inorganic inventory changes suggested that a significant fraction (>50%) of the annual NCP of around 3 mol-C m⁻² yr⁻¹ appeared to be stored within a long-lived organic matter (OM) pool with a lifetime of several months or more. Moreover, transfers into and out of this pool appeared not to be in steady state over the one full seasonal cycle sampled. Accumulation of such a long-lived and potentially C-rich OM pool is suggested to be at least partially responsible for the estimated net air-to-sea CO₂ flux of ~1.3 mol-C m⁻² yr⁻¹ at our study site, while providing a mechanism through which a nutrient-conserving continental shelf pump for CO₂ could potentially operate in this and other similar regions.

1. Introduction

The ocean is an important buffer for atmospheric carbon dioxide (CO_2), naturally storing a large pool of dissolved inorganic carbon (C_T), and also absorbing about a quarter of annual anthropogenic CO_2 emissions (Le Quéré et al., 2009) and thereby mitigating their climatic impacts (IPCC, 2013). The timescale on which the ocean's surface mixed layer equilibrates CO_2 with the atmosphere varies spatially, but is typically from a few months to a year (Broecker and Peng, 1974; Jones et al., 2014). Transfer from the surface to the deep interior is a much slower rate-limiting step, which is performed by the solubility, soft tissue, carbonate and mixed-layer 'pumps' in the open ocean (Volk and Hoffert, 1985; Dall'Olmo et al., 2016). Tsunogai et al. (1999) first proposed the existence of an additional 'continental shelf pump' (CSP) that facilitates C_T transfer from shallow coastal surface waters into the interior ocean, and thereby enhances local oceanic CO_2 uptake. The CSP operates through autotrophic conversion of C_T into organic matter (OM) in a continental shelf sea, which drives a compensatory net air-to-sea CO_2 flux (Chen and Borges, 2009; Chen et al., 2013; Laruelle et al., 2014). In order to prevent the fixed CO_2 from being quickly released back into the atmosphere, the carbon-enriched shelf waters need to be transported into the open ocean, beneath the seasonal thermocline (Tsunogai et al., 1999; Thomas et al., 2004).

The Celtic Sea is a seasonally stratified, temperate sea that forms part of the northwest European continental shelf (Fig. 1). Previous studies of its surface waters have shown that it acts as a net sink of atmospheric CO_2 (Frankignoulle and Borges, 2001; Marrec et al., 2015), which is typical for this type of sea (Borges, 2005; Laruelle et al., 2014). There must therefore be a net flux of carbon (C) out of the shelf sea water column, for example through OM export to sediments, or advective exchange with the open ocean. Celtic Sea sediments could form part of this C sink, as although they predominantly contain sandy material there is some organic matter accumulation (de Haas et al., 2002; Suykens et al., 2011; Diesing et al., 2017). Physical mechanisms that could transport shelf waters into the open ocean have also been identified here (Cooper and Vaux, 1949; Shapiro et al., 2003; Ivanov et al., 2004) and in other similar shelf environments (Álvarez-Salgado et al., 2001). In either case, the question arises of how the nutrient supply is sustained that drives the net C uptake. As essential nutrients such as dissolved inorganic nitrogen and soluble reactive phosphorus (DIN and SRP) are also incorporated into OM, but not replenished through air-sea exchange, the net removal of C_T should be accompanied by a corresponding loss of DIN and SRP from the shelf waters (Thomas et al., 2004; Bozec et al., 2006). Further DIN may be lost from the shelf

waters through denitrification and/or anammox in the shelf sediments (Hydes et al., 2004; Kitidis et al., 2017). Thus, in order to sustain the shelf sea nutrient inventories in the presence of net CO₂ uptake from the atmosphere, any incoming nutrient supply would therefore need to be accompanied by a stoichiometric deficit of carbon relative to outgoing waters. The mechanism by which this occurs remains uncertain. One possibility is that riverine inputs provide high-nutrient, low- C_T waters to the shelf sea. There are also high-nutrient waters in the Irish Sea to the northeast of our study region (Gowen et al., 2002). However, these influences are not thought to be substantial for the Celtic Sea, as on-shelf lateral circulation is relatively slow (Pingree and Le Cann, 1989), and most of the riverine nutrient inputs are quickly removed by biogeochemical processes close to land (Ruiz-Castillo et al., 2017, this issue). Moreover, riverine nutrient inputs to shelf seas tend to be small relative to inputs at the continental margin, for example through upwelling and internal waves at the shelf break (Wollast, 1998). Rivers flowing into the Celtic Sea (e.g. from southern Ireland) also typically have high total alkalinity (A_T) due to chalk and limestone bedrock in their catchments (McGrath et al., 2015). This high A_T supports high C_T concentrations, so the required C deficit relative to nitrogen (N) and phosphorus (P) is unlikely to occur in these waters.

Here, we investigate the hypothesis that OM storage coupled with differences in the stoichiometry of OM remineralisation relative to its production could provide the stoichiometric inconsistency required to sustain the nutrient supply in the Celtic Sea, as has been suggested to occur in similar marine systems (e.g. Álvarez-Salgado et al., 2001; Bozec et al., 2006). This would require the stoichiometric C:N:P ratio for remineralisation to have a lower C coefficient than in the equivalent ratio for net community production (NCP). The shelf nutrient inventory could therefore be sustained through some combination of enhanced remineralisation of non-C nutrients, or the build-up of a stock of C-rich OM that could be transported into the adjacent open ocean prior to complete remineralisation, thereby acting as a nutrient-conserving CO₂ sink. Our approach is to investigate the distributions and inventories of C_T and dissolved inorganic nutrients, which record the integrated effects of NCP and OM remineralisation, along with other processes such as air-sea CO₂ exchange. We use new seasonally resolved C_T and nutrient observations in this way to estimate the annual magnitude and stoichiometry of NCP and remineralisation at a site in the central Celtic Sea. We subsequently infer seasonal and interannual changes in OM inventories and stoichiometry, and consider mechanisms that could support C export while conserving nutrients, and therefore a CSP.

2. Methods

2.1. Research cruises

Seawater samples were collected during 10 research cruises to the Celtic Sea on the UK research ships RRS *Discovery* and RRS *James Cook*, from March 2014 to August 2015 (Supp. Table S1). All of our datasets are freely available from the British Oceanographic Data Centre (www.bodc.ac.uk).

2.1.1. Marine carbonate system

Samples for C_T and A_T were collected via silicone tubing into 250 ml borosilicate glass bottles either from the samplers (Ocean Test Equipment) positioned on a CTD rosette frame, or from the ship's underway seawater supply, following an internationally established protocol (Dickson et al., 2007). Each bottle was sealed shut with a greased ground glass stopper after introducing a 2.5 ml air headspace and sterilising the sample with 50 μ l of saturated mercuric chloride solution. All samples were stored in the dark until analysis.

Measurements of C_T and A_T were carried out at the University of Southampton between June 2014 and January 2016, using several different instruments. The results were calibrated using measurements of batches 128, 135, 136, 138, 141, 142, 144, 146 and 148 of seawater certified reference material (CRM) obtained from A. G. Dickson at Scripps Institution of Oceanography, San Diego, USA (Dickson et al., 2003).

Seawater C_T was measured using either the Versatile INstrument for the Determination of Total inorganic carbon and titration Alkalinity (VINDTA 3C, #024 and #038, Marianda, Germany) or the Dissolved Inorganic Carbon Analyzer AS-C3 (Apollo SciTech Inc., USA). Both of these instruments first acidify a seawater subsample with excess 10% phosphoric acid, to convert all C_T into aqueous CO_2 . Nitrogen gas is then bubbled through to carry the CO_2 to a detector. In the VINDTA 3C, the detection is by coulometric titration (CM5014 CO_2 coulometer, UIC Inc., USA), while the AS-C3 uses infrared absorption (LI-7000 CO_2/H_2O Analyzer, LI-COR, USA). Based on CRM measurements throughout the entire UK-SSB programme, the 1σ precision for C_T was $\pm 2.6 \mu\text{mol kg}^{-1}$ for the VINDTA 3C (number of CRM measurements (n) = 547), and $\pm 4.0 \mu\text{mol kg}^{-1}$ for the Apollo AS-C3 (n = 135).

The A_T was measured using either the VINDTA 3C or the Total Alkalinity Titrator AS-ALK2 (Apollo SciTech Inc., USA). Both instruments determine A_T by an open-cell, potentiometric titration of a seawater subsample with 0.1 M hydrochloric acid. The A_T values from the VINDTA 3C measurements were recalculated using a modified Gran plot approach (Humphreys, 2015a) as implemented by Calkulate v0.1.2 (freely available from <https://github.com/mvdh7/calkulate>). The CRM measurements through the entire UK-SSB programme indicated a 1σ precision for A_T of $\pm 2.7 \mu\text{mol kg}^{-1}$ for the VINDTA 3C ($n = 543$), and $\pm 3.9 \mu\text{mol kg}^{-1}$ for the Apollo AS-ALK2 ($n = 109$).

We performed a cross-over analysis using XOVER v1.0.1 (Humphreys, 2015b), which is freely available from <https://github.com/mvdh7/xover>, to assess our C_T and A_T measurement accuracy relative to historical data in GLODAPv2 (Olsen et al., 2016). This used only data from deeper than 250 m (i.e. off the shelf, beneath the base of the thermocline, and a maximum cross-over distance of 200 km). For C_T , there was a mean \pm standard deviation (SD) offset of $13.6 \pm 7.6 \mu\text{mol kg}^{-1}$ between the combined SSB dataset and nine GLODAPv2 cruises from 1994 to 2008. Despite the large size of this offset, it does not indicate any problem with our measurements, because an ordinary least squares linear regression between the offsets and the sampling date reveal a decrease in offset size at a rate of about $1 \mu\text{mol kg}^{-1} \text{yr}^{-1}$ ($r^2 = 0.66$), corresponding to the anthropogenic C_T increase, and reaching a value of 0 close to the date of the SSB cruises. For A_T , the equivalent offset was $6.8 \pm 7.1 \mu\text{mol kg}^{-1}$ for nine cruises from 1983 to 2008, which is close to the minimum adjustment limit of $6 \mu\text{mol kg}^{-1}$ for this variable in GLODAPv2 (Olsen et al., 2016). In general, cruises closer in time to SSB sampling had a smaller A_T offset. We conclude that our measurements are accurate to within their precision relative to historical observations. Indeed, the internal consistency of data within the GLODAPv2 compilation is reported as ± 4 and $\pm 6 \mu\text{mol kg}^{-1}$ for C_T and A_T respectively (Olsen et al., 2016).

2.1.2. Other variables

Macronutrient samples were collected into 60 ml high density polyethylene (HDPE, Nalgene) bottles that had been aged and acid washed before sampling. The measurements of nitrate, nitrite, ammonium, and soluble reactive phosphorus (SRP) were carried out at sea during the UK-SSB cruises, immediately after sample collection, using the Plymouth Marine Laboratory 5-channel Bran and Luebbe AAIII system, following Woodward and Rees (2001). The instrument was calibrated using in-house nutrient standards, and accuracy was monitored by

regular comparisons with Nutrient Reference Material obtained from KANSO Technos (Japan). We define dissolved inorganic nitrogen (DIN) as the sum of the concentrations of nitrate, nitrite and ammonium. The 1σ precisions were $\pm 0.13 \mu\text{mol kg}^{-1}$ and $\pm 0.0073 \mu\text{mol kg}^{-1}$ for DIN and SRP respectively.

Water column hydrography was measured by Sea-Bird conductivity-temperature-depth (CTD) sensors attached to the sampling rosette frame, to determine the temperature (T in $^{\circ}\text{C}$), practical salinity (S) and depth for each discrete biogeochemical sample. The sea surface hydrography (T and S) was measured continuously by Sea-Bird sensors through the underway seawater supply at a nominal depth of 6 m. The T and S sensor data for both the underway and CTD systems were calibrated using a set of discrete samples collected during each cruise. We consider the 1σ uncertainty in S to be ± 0.002 (Le Menn, 2011). Further information on the sensor measurements and processing can be found in the cruise reports.

2.1.3. Unit conversions

The C_T and A_T measurements were determined in units of $\mu\text{mol kg}^{-1}$, while DIN and SRP were reported in mmol m^{-3} under analysis conditions (i.e. at 20°C). For the column inventory analysis, we converted the C_T , DIN and SRP measurements into units of mmol m^{-3} at the *in situ* temperature. We calculated all densities for these conversions using the Gibbs-SeaWater (GSW) Oceanographic Toolbox v3.05.5 (McDougall and Barker, 2011).

2.2. Central Celtic Sea mooring

A temperature-salinity (TS) chain (a series of sensors positioned vertically along a cable moored to the seafloor) was also deployed on a Cefas SmartBuoy mooring at the Central Celtic Sea site (CCS) from March 2014 to July 2015 (Wihsgott et al., 2016). This measured seawater T and S at a vertical resolution of 2.5 m in the pycnocline and 5-20 m resolution in the surface and bottom layers. The temporal resolution was 5 minutes. A combination of sensor types were used: Star Oddi DST Centi temperature loggers, Star Oddi Starmon mini-underwater temperature recorder and RBRsolo T temperature logger, along with SBE16+ SeaCAT CTD and SBE37 MicroCAT CTD sensors. We calculated mixed layer depth (z_{ml} in m) as the shallowest depth where the potential density increased by 0.02 kg m^{-3} from its value at 10 m.

2.3. Auxiliary datasets

We obtained $0.75^\circ \times 0.75^\circ$ gridded atmospheric/surface ocean reanalysis data at 3-hourly temporal resolution from the ERA-Interim data product (Dee et al., 2011), which is produced by the European Centre for Medium-Range Weather Forecasts (ECMWF). Data were downloaded from ECMWF on 1st August 2016 for the following variables, over the period from 1st March 2014 to 31st December 2015: sea surface temperature (SST in $^\circ\text{C}$), mean sea level pressure (P_{baro} in bar), 10 metre U wind component (U_{10u} in m s^{-1}), 10 metre V wind component (U_{10v} in m s^{-1}), and 2 metre dewpoint temperature (T_{dp} in $^\circ\text{C}$). We calculated the wind speed at 10 m above the sea surface (U_{10} , in m s^{-1}) from its components U_{10u} and U_{10v} .

2.4. Central Celtic Sea site

Most of the analysis presented here was carried out at CCS, which was the most frequently-occupied location during the UK-SSB sampling campaign. All samples collected within a 12 km radius of 49.4°N , 8.54°W were considered to represent CCS (Fig. 1). This radius was selected such that sufficient data were captured to constrain the interior biogeochemical seasonality, whilst deviating as little as possible from the site itself. We then manually grouped the CCS observational dataset based on the sampling date: we selected a set of date boundaries that minimised the width of each time interval, while ensuring that there were enough data within each interval to determine the vertical profile of each biogeochemical variable, resulting in 15 time intervals (Table 1).

Vertical profiles of biogeochemical variables at each site were typically homogeneous during the winter months, and had a two-layer shape during the stratified summer. As such, it was possible to fit error functions to many variables, in order to objectively determine values for each variable in the deep and surface layers, along with the depth of the divide. We thus generated a fit to all data for each variable at each time interval at each site using an equation of the form:

$$v = v_0 + v_1 \operatorname{erf}\left(\frac{z - z_0}{z_1}\right) \quad (1)$$

where v and z are the values and depths respectively of the measurements of each variable, erf is the Gauss error function, and v_0 , v_1 , z_0 and z_1 are coefficients that were adjusted to find the least-squares best fit to these data. These coefficients quantify useful properties: z_0 is the depth of the boundary between the surface and deep layers; z_1 indicates how sharp or diffuse the boundary is, with a smaller value indicating a transition over a narrower depth range; and

the surface and deep layer values of the variable v are given by $(v_0 - v_1)$ and $(v_0 + v_1)$ respectively (see Supp. Table S2 and Supp. Figs. S1–S4).

2.5. Air-sea CO₂ flux

We calculated $p\text{CO}_2^{\text{sw}}$ from the A_T , C_T , S , T , pressure, silicate and SRP observations using version 1.1 of the CO₂SYS program for MATLAB (van Heuven et al., 2011). We calculated Free scale pH in the same way (Supp. Fig. S5). We used the carbonic acid dissociation constants of Lueker et al. (2000), the bisulfate dissociation constant of Dickson (1990) and the boron:chlorinity ratio of Lee et al. (2010). The uncertainties in the input variables resulted in a 1σ precision of $\pm 8.1 \mu\text{atm}$ for calculated $p\text{CO}_2^{\text{sw}}$. Statistical interpolations of these calculated $p\text{CO}_2^{\text{sw}}$ values were limited by low temporal sampling resolution, resulting in key features such as the 2014 spring bloom being partly missed, and therefore inaccurate estimates of the time-integrated air-sea CO₂ flux. We therefore created an empirical algorithm to predict the surface $p\text{CO}_2^{\text{sw}}$ time series at CCS from the reanalysis SST data. The algorithm used different equations for different time periods and SST ranges (Table 2) to account for temporal variation in the surface $p\text{CO}_2^{\text{sw}}$ -SST relationship resulting from changes in biological production and vertical mixing. The mean \pm SD difference between the algorithm-predicted and measured $p\text{CO}_2^{\text{sw}}$ was $-4 \pm 19 \mu\text{atm}$ across all 71 measurements above 25 m depth at CCS, which is similar to the uncertainties quoted for published $p\text{CO}_2^{\text{sw}}$ algorithms in this region (e.g. Marrec et al., 2015).

We obtained measurements of the atmospheric CO₂ dry air mole fraction ($x\text{CO}_2$) for the Greenhouse Gases Reference Network Site at Mace Head, County Galway, Ireland (Dlugokencky et al., 2015). Geographically, this is the closest such observation site to our study area. We applied a piecewise cubic Hermite interpolating polynomial (PCHIP) function (Fritsch and Carlson, 1980; Kahaner et al., 1988) to their monthly mean data to predict $x\text{CO}_2$ in parts per million (ppm) for any given date. We estimated the uncertainty in $x\text{CO}_2$ values interpolated from the monthly means, ± 2.8 ppm, as the standard deviation of the residuals between all of the original individual measurements and the interpolated $x\text{CO}_2$ values at the same time points. We then converted $x\text{CO}_2$ into atmospheric CO₂ partial pressure ($p\text{CO}_2^{\text{atm}}$) using data from the ERA-Interim reanalysis (Dee et al., 2011) at CCS. First, we estimated the water vapour pressure (P_v in bar) from T_{dp} (Alduchov and Eskridge, 1996; Lawrence, 2005):

$$P_v = 610.94 \exp\left[17.625 T_{\text{dp}} / (243.04 + T_{\text{dp}})\right] 10^{-5} \quad (2)$$

263 The atmospheric partial pressure of CO₂ ($p\text{CO}_2^{\text{atm}}$ in μatm) was then given by:

$$264 \quad p\text{CO}_2^{\text{atm}} = x\text{CO}_2 (P_{\text{baro}} - P_v) / 1.01325 \quad (3)$$

265 We calculated the air-sea CO₂ flux (F , in $\mu\text{mol m}^{-2} \text{hr}^{-1}$) following Wanninkhof (2014), using
266 3-hourly resolution data from ECMWF, the algorithm-predicted $p\text{CO}_2^{\text{sw}}$ (Table 2), and
267 $p\text{CO}_2^{\text{atm}}$ calculated from $x\text{CO}_2$ (Eq. 3). The flux equation is:

$$268 \quad F = k \alpha (p\text{CO}_2^{\text{sw}} - p\text{CO}_2^{\text{atm}}) \quad (4)$$

269 where α is the solubility of CO₂, evaluated following Weiss (1974) and converted to units of
270 $\text{mol m}^{-3} \text{atm}^{-1}$ using the GSW toolbox (McDougall and Barker, 2011), and k is the gas
271 transfer velocity in m hr^{-1} :

$$272 \quad k = 0.00251 U_{10}^2 (660/D)^{0.5} \quad (5)$$

273 where D is the dimensionless Schmidt number for CO₂ at the surface layer seawater
274 temperature (Wanninkhof, 2014). The flux calculations were carried out in MATLAB
275 (MathWorks) using the ‘co2flux’ program available from <https://github.com/mvdh7/co2flux>.

276 **2.6. Column inventories**

277 The column inventory of each biogeochemical variable was determined at each time interval
278 by integrating the fitted profile for the variable (in mmol m^{-3}) from the surface to the seafloor
279 depth, taken as the mean seafloor depth across all CCS sampling stations ($Z = 146.9 \text{ m}$). We
280 then attempted to remove the influence of processes other than NCP and remineralisation on
281 the column inventories. To correct for air-sea gas exchange, we subtracted the air-sea CO₂
282 flux integrated between each time point and winter 2014 (C_{atm}) from each time point’s raw C_T
283 inventory. Hydes et al. (2004) suggest a constant denitrification rate of $0.1 \text{ mmol-N m}^{-2} \text{day}^{-1}$
284 for the Celtic Sea. We therefore subtracted the product of this rate and the number of days
285 between each time point and winter 2014 from the DIN inventory at each time point to
286 correct for the potential loss of DIN through denitrification (DIN_{dnf}). Kitidis et al. (2017)
287 more recently reported a similar mean flux of DIN from sediments into the seawater due to
288 denitrification/anammox processes at a site near CCS. Although these authors identified some
289 seasonal variability in this value, but we did not include this in our analysis as it was too
290 small to alter our interpretation and conclusions.

2.7. Uncertainty analysis

The uncertainties in all of the final results, reported as 95% confidence intervals, were calculated using Monte Carlo simulations. Explicitly, we replicated the column inventory analysis 1000 times, each time adding different random offsets to each individual measurement. These offsets were normally distributed, with a SD equal to the 1σ analytical uncertainty for each measurement. The random noise was added both to the measurements of each variable. We report the 95% uncertainty in each column inventory as double the SD of all of its replicates.

2.8. Salinity correlations

We quantified the seasonally changing patterns in C_T , DIN and SRP remineralisation across the Celtic Sea by determining their correlations with practical salinity in the deep layer. For these correlations, we used only data satisfying the following conditions: (1) salinity > 35.2 , to exclude near-coastal waters with nutrient-salinity relationships different from the majority of the shelf; (2a) where seafloor depth < 200 m (i.e. on-shelf), sample depth > 60 m, to exclude the surface layer where DIN and SRP are reduced to virtually zero in the summer months; and (2b) where seafloor depth > 200 m (i.e. off-shelf), 150 m $<$ sample depth < 200 m, again to exclude the surface layer (which was deeper off-shelf) and also deeper waters that were less strongly affected by seasonal remineralisation. The potential density of the off-shelf 150 to 200 m layer throughout the year was similar to the on-shelf winter potential density, supporting our choice of this as the off-shelf endmember for the correlations. Summary statistics for these correlations are provided in Table 3, and scatter plots are shown by Supp. Figs. S12–S14.

3. Results and discussion

3.1. Central Celtic Sea site

3.1.1. Air-sea CO₂ flux

Few studies have examined the Celtic Sea inorganic carbon cycle in detail, but those that have were mostly focused on the surface layer and air-sea CO₂ exchange. Frankignoulle and Borges (2001) used a compilation of surface ocean $p\text{CO}_2^{\text{sw}}$ data to demonstrate that the northwest European continental shelf seas are a net sink for atmospheric CO₂, at a rate between 1.8 and 2.9 mol m⁻² yr⁻¹. This result was quantitatively supported by a more recent model study (Wakelin et al., 2012). However, other studies have found smaller net air-sea CO₂ fluxes for this region. Borges et al. (2006) compiled published datasets across the entire northwest European shelf, and Marrec et al. (2015) generated predictive algorithms for Celtic Sea $p\text{CO}_2^{\text{sw}}$ from variables including sea surface temperature, mixed layer depth and chlorophyll-*a* concentration. These studies agree that the Celtic Sea is a net sink for atmospheric CO₂, but they suggest a typical rate a little under 1 mol m⁻² yr⁻¹. Our analysis also indicated that the CCS site acted as a net atmospheric CO₂ sink: the mean air-to-sea CO₂ flux at CCS from 21st March 2014 (i.e. the start of the UK-SSB sampling period) to the same date in 2015 was 1.3 ± 0.3 mol m⁻² yr⁻¹ (Fig. 2). The magnitude of this flux is consistent with previous Celtic Sea studies, although it is towards their lower end. A separate analysis of *in situ* CO₂ uptake (photosynthesis) and production (plankton respiration) data also found that CCS was a net atmospheric CO₂ sink, as primary production was typically greater than community respiration (García-Martín et al., 2017, this issue).

The $\Delta p\text{CO}_2$ was vertically uniform and close to atmospheric equilibrium during March-April. Its seasonal pattern was similar to C_T , with CO₂ undersaturation in the surface layer during the spring-summer. The surface $p\text{CO}_2^{\text{sw}}$ variability was dominated by biological C_T uptake and release, rather than seasonal seawater heating and cooling, which would have been expected to induce an increase in $p\text{CO}_2^{\text{sw}}$ (and therefore $\Delta p\text{CO}_2$) during the warmer summer months. Indeed, the amplitude of the SST seasonal cycle was about 10°C. Alone, this would have driven a winter-summer $p\text{CO}_2^{\text{sw}}$ increase of about 200 µatm (Takahashi et al., 2009), whereas we observed a c. 85 µatm decline during this period (Fig. 2a). Other factors that could affect the $\Delta p\text{CO}_2$ cycle are atmospheric $p\text{CO}_2$, and seawater A_T . The amplitude of seasonal atmospheric $p\text{CO}_2$ cycle was an order of magnitude smaller than that of $p\text{CO}_2^{\text{sw}}$, while A_T was not noticeably affected by seasonal stratification, remaining relatively

homogeneous both laterally and vertically throughout the Celtic Sea for the duration of the SSB sampling campaign (Supp. Fig. S8). The seasonal variability of atmospheric $p\text{CO}_2$ and A_T therefore did not significantly influence that of $\Delta p\text{CO}_2$.

The algorithm that we created to predict surface $p\text{CO}_2^{\text{sw}}$ (Table 2) produced an annual range of about 85 μatm , similar to previous studies (e.g. Marrec et al., 2015). However, there were differences in the seasonal pattern. Firstly, we found that the $p\text{CO}_2^{\text{sw}}$ had two distinct minima during 2014, first in May-June and then a weaker minimum in November-December associated with an autumn phytoplankton bloom (Wihsgott et al., 2017, this issue). Our 2015 data end too early in the seasonal cycle to determine whether these dual minima were repeated. Secondly, Marrec et al. (2015) projected that $\Delta p\text{CO}_2$ should be positive for approximately a third of each year, during the winter months, reaching values up to about 30 μatm . However, neither our algorithm nor our observations indicate such consistently high $\Delta p\text{CO}_2$ values. We did not collect any carbonate chemistry samples between November and March, so we cannot be certain which is correct. However, the observational $p\text{CO}_2^{\text{sw}}$ data from SOCAT (Bakker et al., 2016) used by Marrec et al. (2015) to test their algorithm were in atmospheric equilibrium during this season, rather than supersaturated as predicted, for about half of the years that they considered. This winter supersaturation may therefore be an intermittent phenomenon, but our dataset is unable to identify whether it occurred between 2014 and 2015.

The most uncertain part of our air-sea CO_2 flux algorithm was between autumn 2014 and winter 2015, due to a lack of observations during that period. Comparison of the pattern of $p\text{CO}_2^{\text{sw}}$ (Fig. 2a) with other studies (e.g. Marrec et al., 2015) and our understanding of marine carbonate system drivers suggests that the $p\text{CO}_2^{\text{sw}}$ predicted by the algorithm for this period is likely to underestimate the true value. Consequently, we consider the air to sea CO_2 flux calculated for this period as a maximum estimate.

3.1.2. Inorganic inventory changes

Vertical profiles of C_T , DIN, SRP and related hydrographic variables were constrained at two roughly equivalent time points both in 2014 and 2015, referred to as ‘winter’ (i.e. March-April, pre-spring bloom) and ‘summer’ (August). Between these, there was a single ‘late spring’ profile in June 2014, and a series of ‘in-bloom’ profiles (April-May) captured the progression of the 2015 spring bloom at a relatively high temporal resolution, followed by an ‘early spring’ profile in May 2015. There was an ‘autumn’ (November) profile in 2014 only.

Direct comparisons between the two years can therefore be drawn from comparing winter and summer, while the additional points can be used to more finely resolve the seasonal changes.

The TS chain measurements clearly illustrate the seasonal cycle of surface warming and stratification followed by winter mixing (Fig. 3a). The CCS site was vertically mixed during the winter, but physical and biogeochemical variables exhibited a two-layer stratified structure during the spring and summer. Most variables were vertically homogeneous in winter each year, after which C_T , DIN and SRP declined strongly in the surface layer (i.e. shallower than 40-50 m) through the spring and summer (Fig. 3b-d), through drawdown associated with NCP. DIN reached virtually zero (i.e. beneath the detection limit of ~ 0.02 mmol m^{-3}), while SRP declined to a minimum of about 0.05 mmol m^{-3} , consistent with previous studies that have identified DIN as the limiting nutrient in this region (e.g. Davis et al., 2014). The concentrations of these variables increased in the deep layer over the same period, consistent with remineralisation of sinking OM. Stratification began to break down towards the autumn, and the water column was reset to a vertically homogeneous state by the following winter.

The dominant control on the vertical density structure in the Celtic Sea is temperature (Pingree et al., 1976). Salinity thus only constitutes a second-order control, and it was less variable throughout the seasonal cycle. However, the vertical partitioning of the water column due to seasonal stratification did facilitate a notable increase in salinity from August to December 2014 in the bottom mixed layer only (Fig. 3e). This suggests that open ocean waters increased in influence relative to on-shelf waters during this time, as no *in situ* processes can modify deep layer S to this extent. The DIN and SRP increased disproportionately in the deep layer (i.e. beneath c. 50 m) during the same period (Fig. 3c-d), suggesting that increasing nutrient concentrations relative to C_T at this time may have been associated with the advective flux that elevated S , rather than *in situ* OM remineralisation. In support, Ruiz et al. (2017, this issue) describe a shelf-wide estuarine-type circulation that advects saline, nutrient-rich waters on to the shelf during the stratified summer months. They estimate that 70-80% of the increase in deep layer DIN observed at CCS since the fully mixed winter state could be supplied by this physical transport mechanism.

3.1.3. Production and remineralisation

During the first half of each year, when stratification was increasing, changes in C_T , DIN and SRP profiles between successive time points can reveal the depth ranges over which NCP and net remineralisation occurred (e.g. Fig. 4). For intervals when surface layer concentrations declined, the average NCP rate can therefore be estimated by integrating the change in C_T only over the depth range where C_T declined and correcting the result for air-sea CO_2 exchange, which can be assumed to affect only the surface layer when the water column is stratified. Similarly, deep layer increases in C_T can be attributed to remineralisation. The same procedure can be carried out for DIN and SRP, with the remineralisation calculation for DIN corrected for denitrification and/or anammox (Hydes et al., 2004; Kitidis et al., 2017), and no gas exchange correction (Table 4). The main spring bloom in 2014 resulted in a mean NCP of $35.9 \pm 2.3 \text{ mmol-C m}^{-2} \text{ d}^{-1}$ from winter to late spring, which is consistent with an NCP estimate for the seasonally-stratified North Sea of 16-46 $\text{mmol m}^{-2} \text{ d}^{-1}$ for this season (Bozec et al., 2006). This represents a total of $3.08 \pm 0.20 \text{ mol-C m}^{-2}$ C_T conversion into OM since the mixed winter state, integrated over the period between our winter and late spring 2014 time points (i.e. 86 days; Table 1). The equivalent DIN and SRP drawdowns were $342 \pm 7 \text{ mmol m}^{-2} \text{ d}^{-1}$ (Fig. 4a) and $20.74 \pm 0.36 \text{ mmol m}^{-2} \text{ d}^{-1}$ respectively, resulting in an overall C:N:P for NCP of about 117:13.0:0.79. Corresponding remineralisation of C_T , DIN and SRP within the subsurface layer was $0.78 \pm 0.50 \text{ mol m}^{-2}$, $85 \pm 73 \text{ mmol m}^{-2}$ and $8 \pm 99 \text{ mmol m}^{-2}$, with C:N:P therefore 117:12.7:1.24. This indicates that 20–40% of the NCP was remineralised within the sub-surface (presumably following sinking of the corresponding OM), while 60–80% must have remained within some OM pool, assuming negligible net advection (Pingree and Le Cann, 1989; Brown et al., 2003). The spring bloom period was followed by much weaker NCP and net water column remineralisation from late spring to summer, and then vertical mixing into the autumn and winter (Fig. 4b-c), during which period the decline in deep layer C_T was due to mixing with low- C_T surface waters, not NCP.

The spring bloom of the following year was sampled at higher temporal resolution, during cruise DY029 in April 2015. From winter to early spring 2015 (i.e. 61 days; Table 1), the mean NCP determined from C_T profiles and air-sea CO_2 exchange was $30.5 \pm 2.3 \text{ mmol-C m}^{-2} \text{ d}^{-1}$, comparable to the previous year, estimates from nearby similar regions (Bozec et al., 2006), and the mean NCP of $31 \pm 24 \text{ mmol-C m}^{-2} \text{ d}^{-1}$ (photosynthetic quotient of 1.4) determined at CCS from oxygen-to-argon ratio (O_2/Ar) measurements during this cruise (Seguro et al., 2017, this issue). This NCP integrated from the winter to early spring 2015

time points (i.e. 139 days; Table 1) represented $1.86 \pm 0.14 \text{ mol-C m}^{-2}$ of OM production, compared with $3.08 \pm 0.20 \text{ mol-C m}^{-2}$ for the roughly equivalent period (winter to *late* spring) in 2014. However, further NCP from early spring to summer in 2015 brought the total NCP since winter to $3.30 \pm 0.13 \text{ mol-C m}^{-2}$, similar to the total value for the part of 2014 with positive NCP. The corresponding DIN- and SRP-derived values (from winter to summer 2015) were 343.4 ± 3.9 and $20.86 \pm 0.22 \text{ mmol m}^{-2}$ respectively, resulting in a C:N:P for NCP of about 117:12.2:0.74, similar to the previous year (i.e. 117:13.0:0.79), but with lower N and P coefficients in 2014, or equivalently more C-rich OM production relative to typically assumed (Redfield, 1934; Redfield et al., 1963) and measured (Anderson and Sarmiento, 1994) ratios. Therefore the total amount of OM generated through NCP appeared to be similar during the spring bloom each year, although this may have occurred more rapidly during 2014. Consequently, although the winter and summer time points were at a very similar time for both years, it may be more appropriate to compare ‘winter to late spring 2014’ with ‘winter to summer 2015’. Remineralisation from winter to summer 2015 occurred at a C:N:P of 117:11.7:0.88, and represented 24–35% of NCP, in both ways similar to 2014. Both the production and remineralisation of OM were C-rich relative to the likely limiting nutrient, with C:N ranging from 9 to 10 compared with typical values of 6.6 to 7.3 (Redfield, 1934; Redfield et al., 1963; Anderson and Sarmiento, 1994).

3.1.4. Total column inventories

The preceding section’s approach of separating surface NCP from deep remineralisation was less useful from summer onwards, once stratification had begun to break down. At this time, both surface and deep layer C_T and nutrient inventories were influenced by vertical mixing, along with remineralisation throughout the water column. It is therefore more appropriate to consider changes in the total inventories integrated vertically across the entire water column. Remineralisation of both C_T and nutrients continued after summer 2014, first with apparent excess DIN generation until autumn 2014, and then excess C_T until winter 2015 (Fig. 5a-b). We note that the excess N period coincides with the previously-noted apparent advective flux of high salinity to CCS, high DIN waters in the deep layer, so this may have driven the unexpected and transient high DIN, rather than remineralisation (Fig. 5c). However, this high S water had disappeared by winter 2015, due to vertical mixing and shut-down of the summer estuarine-type circulation (Ruiz-Castillo et al., 2017, this issue). The overall trajectory from summer 2014 to winter 2015 is therefore probably representative of net remineralisation, presumably ongoing from some long-lived OM pool.

From late spring 2014 to winter 2015, remineralisation returned a further 2.17 ± 0.43 mol-C m^{-2} C_T , 169 ± 50 mmol-N m^{-2} DIN and 3.27 ± 0.88 mmol-P m^{-2} SRP to the water column, corresponding to a C:N:P ratio of 117:9.1:0.2, with substantially lower N and P coefficients and hence higher C:N and C:P than the NCP stoichiometry. Adding the additional apparent late year remineralisation to that experienced in the deep layer from winter to late spring 2014 resulted in an overall remineralisation C:N:P of 117:10.0:0.5. This corresponded to 96 ± 22 %, 72 ± 26 % and 56 ± 47 % of the OM production of C_T , DIN and SRP respectively in the 2014 spring bloom being remineralised by winter 2015. Thus, acknowledging the potential for advection to complicate our interpretation (see Section 3.2.2), approximately the same amount of C_T that was biologically fixed in the 2014 spring bloom appeared to have been remineralised by winter 2015, while only about three-quarters of the fixed DIN and half of the fixed SRP were remineralised over the same period, noting that the uncertainty in the SRP value is too great for us to speculate about it further. Such a result is difficult to reconcile with the expected behaviours of C, N and P during OM remineralisation (Hopkinson et al., 1997), thus we speculate that this may actually indicate the remineralisation of a C-rich OM pool carried over from before our first W14 sampling point. Furthermore, the air-sea CO_2 flux value that was used to correct these inventories was likely an overestimate from autumn 2014 to winter 2015 (Section 3.1.1). The C_T result is therefore a minimum estimate, and it is possible that more C_T was remineralised than was produced by NCP that year at CCS.

The total water column inventories indicate that the shelf was not operating in steady state from winter 2014 to 2015. The winter inventories of DIN and SRP were 10.3 ± 1.4 % and 10.6 ± 1.1 % lower respectively in 2015 compared to 2014, while that of C_T was 0.36 ± 0.18 % higher (Fig. 5a). The equal (or slightly greater) OM formation during the 2015 spring-summer relative to 2014 was therefore unexpected, because lower nutrient concentrations at the end of the winter mixed state should have supported less NCP. As NCP was the ultimate driver of CO_2 uptake, we would also have expected a lower air-to-sea CO_2 flux following these lower winter nutrient concentrations. This did not occur, because the nutricline was about 10-15 m deeper in 2015 (Fig. 6a), resulting in a greater total N_T conversion into OM despite its lower initial concentration, and matching the behaviour of the thermocline (Fig. 6b). There does not appear to be an obvious mechanism that would drive a deeper nutricline at times of lower surface nutrient concentrations, which would lead summer

NCP to be generally consistent across different years. Rather, it appears to be a coincidence that these phenomena balanced each other out for the two years that we observed.

3.1.5. *Organic matter stoichiometry*

Overall mass balance dictates that changes in the OM composition should mirror the changes in the inorganic inventories (corrected for gas exchange and denitrification/anammox). In Fig. 5b, trajectories between adjacent sampling points that trend towards the bottom right (low C_T , high DIN or SRP) thus indicate the on-shelf generation of relatively C-rich OM, while trajectories that tend towards the top left (high C_T , low DIN or SRP) indicated more N-rich (and/or P-rich) OM generation, relative to an assumed 'typical' C:N:P of 117:16:1 (Anderson and Sarmiento, 1994). The high resolution samples from during the 2015 spring bloom therefore suggest that NCP may have begun with N- and P-rich OM formation, before switching to more C-rich production once surface layer DIN concentrations fell close to zero (Fig. 5b). As mentioned above, the overall change from spring to summer 2015 was similar to the C:N:P uptake stoichiometry observed for the same period in 2014. However, from early spring to summer 2015 we saw the opposite pattern than during the similar period in 2014: the OM became more C-rich. This change to seawater C_T loss with no nutrient loss (as opposed to loss of both to OM following a constant stoichiometry) coincided approximately with CCS surface DIN concentrations approaching zero. We suggest that the C_T loss was therefore a result of continued NCP and OM formation, but that this was using regenerated DIN within the surface layer as its N source rather than drawing from the inorganic pool, which was by then locked away by stratification in the deep layer, as has been observed in the North Sea (Bozec et al., 2006). Although this process should therefore have generated an increasingly C-rich OM pool, presumably associated with more rapid N than C remineralisation from the OM pool, it was not sufficient to return to the original winter 2014 C:N:P stoichiometry. These predicted changes in the OM composition are broadly in agreement with the pattern observed by direct OM stoichiometric measurements at CCS (Davis et al., 2017, this issue), although our approach is not able to distinguish between the dissolved and particulate OM pools.

3.2. Celtic Sea transect

3.2.1. Stratification across the Celtic Sea

In addition to the CCS site, we sampled a northeast-southwest transect across the Celtic Sea during each UK-SSB cruise (Fig. 1). Analysis of these measurements adds a third dimension (i.e. distance from the open ocean) to our so far two-dimensional analysis (i.e. depth and time), highlighting some additional caveats, sources of uncertainty and broader context. Hartman et al. (2017, this issue) describe surface layer UK-SSB measurements from across the entire northwest European continental shelf, thus providing further context.

The pattern of winter mixing followed by surface layer uptake of C_T , DIN and SRP and their increase in the deep layer was consistent across the entire Celtic Sea transect (Fig. 7).

However, the deep layer experienced greater increases in these variables (and others such as ΔpCO_2) further away from the open ocean, although this was reduced for DIN by denitrification/anammox in the seafloor sediments (Hydes et al., 2004; Kitidis et al., 2017). The depth of the surface layer (as defined by the nutricline, 40-50 m) remained relatively constant across the transect while the seafloor became shallower towards the land, so the greater deep layer concentrations could simply indicate that the same amount of NCP had been remineralised, but spread over a narrower deep layer, consistent with the limiting factor for total remineralisation within the deep layer being some function of the OM supply. In addition, the increasing deep layer C_T and nutrients away from the open ocean could reflect the fact that deep waters further from the open ocean had experienced a longer transit time across the shelf within the estuarine-type circulation (Ruiz-Castillo et al., 2017, this issue), and thus greater accumulation of sinking organic matter from the surface layer, in a manner analogous to how nutrient concentrations tend to increase along isopycnals away from the surface in the open ocean (Takahashi et al., 1985).

The increasing strength of biogeochemical stratification moving away from the open ocean has important implications for interpreting our results from CCS, which lay towards the open ocean end of the Celtic Sea transect. For example, the surface layer air-sea CO_2 disequilibrium during the stratified period increased away from the open ocean. We would therefore expect the Celtic Sea as a whole to exhibit a greater net air-sea CO_2 flux than that calculated for the CCS site, which was relatively close to the open ocean end of the transect. This is consistent with our CCS air-sea CO_2 flux estimate falling towards the lower end of

previously published results (Section 3.1.1). A second example concerns potential advective fluxes within the Celtic Sea, as discussed in the following section.

3.2.2. Biogeochemical relationships with salinity

In the Celtic Sea, S acts as a tracer of the relative influence of open ocean and shelf waters, particularly in the deep mixed layer beneath the pycnocline, where no other processes can modify it. Throughout the year, S decreases moving on to the shelf, ultimately as a result of dilution by riverine inputs. During the winter, S was vertically homogeneous at each point across the shelf, while the isohalines were tilted away from vertical towards the open ocean in the surface during the summer (i.e. increasing S with depth, Fig. 7h). This suggests that there was likely a net transport of relatively fresh waters towards the open ocean in the surface layer, and a net transport of salt towards the land within the bottom mixed layer at CCS during the summer. During the winter, while C_T and SRP were laterally homogeneous, DIN was correlated with salinity (Table 3) and declined away from the open ocean (Figs. 7d and 8b). There were no relationships between S and any of C_T , DIN or SRP in the surface layer during the summer months, when NCP was the dominant control on these biogeochemical variables. However, correlations could be identified in the deep layer throughout the seasonal cycle, which were variable through time, but fairly consistent with each other (Fig. 8, Table 3). These relationships with S indicated that C_T and SRP were enriched on the shelf relative to the open ocean during the summer months, and returned close to open-ocean values during the winter, consistent with a seasonal cycle of remineralisation and vertical mixing. Although the DIN- S relationship had a similar pattern to those for C_T and SRP, there was a significant offset from the values predicted from the SRP relationship and an assumed N:P stoichiometry of 16:1 (Fig. 8b). This offset was positive, with a mean value of $7.5 \pm 2.1 \text{ mmol m}^{-3}$ per unit practical salinity, indicating that the shelf waters were virtually always depleted in DIN relative to the open ocean, likely as the result of denitrification and/or anammox in the shelf sediments (Hydes et al., 2004; Kitidis et al., 2017).

The preceding interpretation of the changing C_T and nutrient vertical profiles at CCS mostly ignored the possibility of advective influences. However, given the changing deep layer C_T and nutrient concentrations in the stratified period, advection of water from another part of the shelf could generate an apparent increase or decrease in remineralisation at CCS. As well as directly changing the inorganic inventories, this could also supply OM to CCS that had originally formed elsewhere on the shelf, particularly given our evidence that a significant

fraction of NCP (>50%) remained within the OM pool, as opposed to the deep layer remineralised pool, over seasonal timescales (Fig. 5). Significant advection of a cross-shelf OM gradient would hence introduce uncertainties into our one-dimensional estimates of the fraction of NCP that had been remineralised. Indeed, production and advection of a long-lived OM pool could provide a source for the possible excess of remineralisation over NCP that we observed from winter 2014 to winter 2015 at CCS. It is also important to note that we cannot determine how CCS could have been affected by any advective fluxes of material perpendicular to the Celtic Sea transect that we sampled, which could have a different relationship with S than observed along the UK-SSB transect. However, in general we do not expect this to have significantly affected our results, because previous studies have found that water exchange between the Celtic Sea and adjacent open ocean is relatively slow (Holt et al., 2009; Huthnance et al., 2009), as is net lateral circulation on the shelf itself (Pingree and Le Cann, 1989), with water taking about 2 years to reach the central Celtic Sea after entering the shelf from the open ocean (Hydes et al., 2004).

The Celtic Sea transect dataset also indicates that the increase in C_T observed at CCS from winter 2014 to winter 2015, and the simultaneous declines in DIN and SRP, were not a result of spatial variability. As these biogeochemical variables appeared to diverge from their open ocean values moving into the shelf sea (Fig. 8), apparent changes at a static site such as CCS could be caused by advective reorganisation of the water on the shelf, with a greater or lesser open ocean influence at CCS in different years. If this were the case, then the apparent nutrient loss that we observed could simply be an artefact of the spatial variability, rather than a temporal biogeochemical trend. However, it appears that the changes in C_T , DIN and SRP that we observed at CCS over this time period were consistent throughout most of S range observed across the Celtic Sea transect (Fig. 9). This therefore supports our earlier interpretation that the seasonal biogeochemical changes observed at CCS were representative of processes operating across the wider Celtic Sea.

Finally, our transects indicated that the shelf A_T was relatively homogeneous both spatially and temporally throughout the UK-SSB sampling campaign (Fig. 7i; Supp. Fig. S8), with a weakly positive relationship with salinity. At CCS, we observed no low A_T excursions from the A_T -salinity relationship that could be evidence for pelagic calcification, for example by coccolithophores (Suykens et al., 2010), confirming that our calculated water column inventories of C_T at CCS were not significantly affected by such processes during the UK-SSB sampling period.

3.2.3. *Nutrient-conserving mechanism*

Our estimated net oceanic CO₂ uptake of $>1 \text{ mol-C m}^{-2} \text{ yr}^{-1}$ within the Celtic Sea suggests that an active CSP operates within this system. Given the preceding presented data and analysis, we suggest two mechanisms through which such a CSP could operate in a nutrient-conserving manner, i.e. without a significant external nutrient-rich source from rivers, and without the shelf becoming depleted in these nutrients over time, as follows.

Firstly, we saw an increase in vertically-integrated C_T at CCS from winter 2014 to winter 2015, along with a simultaneous decline in DIN and SRP (Fig. 5a). The initial winter 2014 values of C_T , DIN and SRP were relatively close to the base of the thermocline in the adjacent open ocean, suggesting that there may recently have been relatively strong water exchange across the shelf break, which did not occur again during our sampling period. If the shelf sea were to follow a cycle of increasing C_T while DIN and SRP declined between these irregular ‘flushing’ events, then the exchange of shelf waters with the open ocean would constitute a net export of C_T while DIN and SRP were replenished.

Secondly, as previously identified in similar environments (e.g. Butler et al., 1979; Johnson et al., 2013), it appears that a substantial fraction ($>50\%$) of the OM produced during the spring bloom each year was only slowly remineralised over many months (Fig. 5). Indeed, evidence that deep layer advective transport could have accounted for 70-80% of the DIN increase at CCS from winter to summer each year (Ruiz-Castillo et al., 2017, this issue) suggests that our calculated fraction of OM that was not remineralised is a minimum estimate, so the long-lived OM pool could be greater still. Moreover, the non-steady state situation that we observed over the 1.5 sampled years further suggests that some fraction of this (semi-)refractory OM pool was potentially not remineralised within the same year and hence may play a role in redistributing C and nutrients within the Celtic Sea itself (Fig. 7). We therefore speculate that this long-lived OM pool could also function to export C from the shelf sea into the open ocean, for example during exchange with off-shelf waters with a lower OM concentration.

Future synthesis of the inorganic measurements presented here along with OM concentration and stoichiometry datasets collected during the UK-SSB research programme in the context of a system which likely operates on a multi-annual timescale will be required to assess the capacity of these possible mechanisms to sustain a nutrient-conserving CSP in temperate, seasonally stratified continental shelf seas like the Celtic Sea.

4. Conclusions

The Celtic Sea experiences seasonal physical and biogeochemical stratification with low C_T and nutrient concentrations driving a net air to sea CO_2 flux, while remineralisation increases these concentrations in the deep layer. Repeated observations at the CCS site suggest that the inventories of DIN and SRP declined by about 10% from winter 2014 to winter 2015, while C_T increased. Transect data indicate that these temporal changes observed at CCS were consistent across much of the Celtic Sea, rather than being an artefact of advection and spatial variability. Lower availability of nutrients for NCP in 2015 was compensated by a deeper nutricline, so there was no reduction in either the total amount of NCP or air-sea CO_2 exchange during the subsequent spring bloom. Analysis of stoichiometry during nutrient uptake for NCP and remineralisation indicated the production of C-rich OM. However, some fraction of the OM generated on the shelf appears to not have been remineralised within the year it was created, suggested that a long-lived stock of OM could accumulate in the shelf waters. This, and the overall changes in inorganic inventories that we observed, could provide alternative mechanisms through which a nutrient-conserving CSP could operate, both in the Celtic Sea and in other seasonally stratified, temperate continental shelf seas.

5. Acknowledgements

We thank the officers, crew and scientists involved with all UK-SSB cruises on the RRS *Discovery* and RRS *James Cook*, in particular the carbonate chemistry samplers including C. Kivimäe, L. Darroch, J. Fox, R. Houlding, P. Nelson, N. Hicks, A. Poulton, K. Mayers and R. Sims. We thank I. Seguro, E. Ruiz-Castillo, E. García-Martín and C. Davis for useful discussions. This study was funded by the Natural Environment Research Council (UK) through “CaNDyFloSS: Carbon and Nutrient Dynamics and Fluxes over Shelf Systems” grants NE/K002058/1 to EMSW, NE/K001701/1 to JEH and SEH, and NE/K00185X/1 to CMM and EPA.

6. References

- Alduchov, O.A., Eskridge, R.E., 1996. Improved Magnus Form Approximation of Saturation Vapor Pressure. *J. Appl. Meteor.* 35, 601–609. doi:10.1175/1520-0450(1996)035<0601:IMFAOS>2.0.CO;2
- Álvarez-Salgado, X.A., Doval, M.D., Borges, A.V., Frankignoulle, M., Woodward, E.M.S., Figueiras, F.G., 2001. Off-shelf fluxes of labile materials by an upwelling filament in the NW Iberian Upwelling System. *Prog. Oceanogr.* 51, 321–337. doi:10.1016/S0079-6611(01)00073-8
- Anderson, L.A., Sarmiento, J.L., 1994. Redfield ratios of remineralization determined by nutrient data analysis. *Global Biogeochem. Cy.* 8, 65–80. doi:10.1029/93GB03318
- Bakker, D.C.E., Pfeil, B., Landa, C.S., Metzl, N., O'Brien, K.M., Olsen, A., Smith, K., Cosca, C., Harasawa, S., Jones, S.D., Nakaoka, S.-I., Nojiri, Y., Schuster, U., Steinhoff, T., Sweeney, C., Takahashi, T., Tilbrook, B., Wada, C., Wanninkhof, R., Alin, S.R., Balestrini, C.F., Barbero, L., Bates, N.R., Bianchi, A.A., Bonou, F., Boutin, J., Bozec, Y., Burger, E.F., Cai, W.-J., Castle, R.D., Chen, L., Chierici, M., Currie, K., Evans, W., Featherstone, C., Feely, R.A., Fransson, A., Goyet, C., Greenwood, N., Gregor, L., Hankin, S., Hardman-Mountford, N.J., Harlay, J., Hauck, J., Hoppema, M., Humphreys, M.P., Hunt, C.W., Huss, B., Ibáñez, J.S.P., Johannessen, T., Keeling, R., Kitidis, V., Körtzinger, A., Kozyr, A., Krasakopoulou, E., Kuwata, A., Landschützer, P., Lauvset, S.K., Lefèvre, N., Lo Monaco, C., Manke, A., Mathis, J.T., Merlivat, L., Millero, F.J., Monteiro, P.M.S., Munro, D.R., Murata, A., Newberger, T., Omar, A.M., Ono, T., Paterson, K., Pearce, D., Pierrot, D., Robbins, L.L., Saito, S., Salisbury, J., Schlitzer, R., Schneider, B., Schweitzer, R., Sieger, R., Skjelvan, I., Sullivan, K.F., Sutherland, S.C., Sutton, A.J., Tadokoro, K., Telszewski, M., Tuma, M., van Heuven, S.M.A.C., Vandemark, D., Ward, B., Watson, A.J., Xu, S., 2016. A multi-decade record of high-quality $f\text{CO}_2$ data in version 3 of the Surface Ocean CO_2 Atlas (SOCAT). *Earth Syst. Sci. Data* 8, 383–413. doi:10.5194/essd-8-383-2016
- Borges, A.V., 2005. Do we have enough pieces of the jigsaw to integrate CO_2 fluxes in the coastal ocean? *Estuaries* 28, 3–27. doi:10.1007/BF02732750
- Borges, A.V., Schiettecatte, L.-S., Abril, G., Delille, B., Gazeau, F., 2006. Carbon dioxide in European coastal waters. *Estuar. Coast. Shelf S.* 70, 375–387. doi:10.1016/j.ecss.2006.05.046
- Bozec, Y., Thomas, H., Schiettecatte, L.-S., Borges, A.V., Elkalay, K., de Baar, H.J.W., 2006. Assessment of the processes controlling the seasonal variations of dissolved inorganic carbon in the North Sea. *Limnol. Oceanogr.* 51, 2746–2762. doi:10.4319/lo.2006.51.6.2746
- Broecker, W.S., Peng, T.-H., 1974. Gas exchange rates between air and sea. *Tellus* 26, 21–35. doi:10.3402/tellusa.v26i1-2.9733
- Brown, J., Carrillo, L., Fernand, L., Horsburgh, K.J., Hill, A.E., Young, E.F., Medler, K.J., 2003. Observations of the physical structure and seasonal jet-like circulation of the Celtic Sea and St. George's Channel of the Irish Sea. *Cont. Shelf Res.* 23, 533–561. doi:10.1016/S0278-4343(03)00008-6
- Butler, E.I., Knox, S., Liddicoat, M.I., 1979. The relationship between inorganic and organic nutrients in sea water. *J. Mar. Biol. Assoc. U.K.* 59, 239–250. doi:10.1017/S0025315400046312
- Chen, C.-T.A., Borges, A.V., 2009. Reconciling opposing views on carbon cycling in the coastal ocean: Continental shelves as sinks and near-shore ecosystems as sources of atmospheric CO_2 . *Deep-Sea Res. Pt II* 56, 578–590. doi:10.1016/j.dsr2.2009.01.001

- Chen, C.-T.A., Huang, T.-H., Chen, Y.-C., Bai, Y., He, X., Kang, Y., 2013. Air–sea exchanges of CO₂ in the world’s coastal seas. *Biogeosciences* 10, 6509–6544. doi:10.5194/bg-10-6509-2013
- Cooper, L.H.N., Vaux, D., 1949. Cascading Over the Continental Slope of Water from the Celtic Sea. *J. Mar. Biol. Ass. U.K.* 28, 719–750. doi:10.1017/S0025315400023547
- Dall’Olmo, G., Dingle, J., Polimene, L., Brewin, R.J.W., Claustre, H., 2016. Substantial energy input to the mesopelagic ecosystem from the seasonal mixed-layer pump. *Nature Geosci.* 9, 820. doi:10.1038/ngeo2818
- Davis, C.E., Blackbird, S., Wolff, G., Woodward, M., Mahaffey, C., 2017. Seasonal organic matter dynamics in a temperate shelf sea. *Prog. Oceanogr.* in review.
- Davis, C.E., Mahaffey, C., Wolff, G.A., Sharples, J., 2014. A storm in a shelf sea: Variation in phosphorus distribution and organic matter stoichiometry. *Geophys. Res. Lett.* 41, 2014GL061949. doi:10.1002/2014GL061949
- de Haas, H., van Weering, T.C.E., de Stigter, H., 2002. Organic carbon in shelf seas: sinks or sources, processes and products. *Cont. Shelf Res.* 22, 691–717. doi:10.1016/S0278-4343(01)00093-0
- Dee, D.P., Uppala, S.M., Simmons, A.J., Berrisford, P., Poli, P., Kobayashi, S., Andrae, U., Balmaseda, M.A., Balsamo, G., Bauer, P., Bechtold, P., Beljaars, A.C.M., van de Berg, L., Bidlot, J., Bormann, N., Delsol, C., Dragani, R., Fuentes, M., Geer, A.J., Haimberger, L., Healy, S.B., Hersbach, H., Hólm, E.V., Isaksen, L., Kållberg, P., Köhler, M., Matricardi, M., McNally, A.P., Monge-Sanz, B.M., Morcrette, J.-J., Park, B.-K., Peubey, C., de Rosnay, P., Tavolato, C., Thépaut, J.-N., Vitart, F., 2011. The ERA-Interim reanalysis: configuration and performance of the data assimilation system. *Q. J. R. Meteorol. Soc.* 137, 553–597. doi:10.1002/qj.828
- Dickson, A.G., 1990. Standard potential of the reaction: $\text{AgCl}_{(s)} + 0.5 \text{H}_{2(g)} = \text{Ag}_{(s)} + \text{HCl}_{(aq)}$, and the standard acidity constant of the ion HSO_4^- in synthetic sea water from 273.15 to 318.15 K. *J. Chem. Thermodyn.* 22, 113–127. doi:10.1016/0021-9614(90)90074-Z
- Dickson, A.G., Afghan, J.D., Anderson, G.C., 2003. Reference materials for oceanic CO₂ analysis: a method for the certification of total alkalinity. *Mar. Chem.* 80, 185–197. doi:10.1016/S0304-4203(02)00133-0
- Dickson, A.G., Sabine, C.L., Christian, J.R. (Eds.), 2007. Guide to best practices for ocean CO₂ measurements. *PICES Special Publication* 3.
- Diesing, M., Kröger, S., Parker, R., Jenkins, C., Mason, C., Weston, K., 2017. Predicting the standing stock of organic carbon in surface sediments of the North–West European continental shelf. *Biogeochemistry* 1–18. doi:10.1007/s10533-017-0310-4
- Dlugokencky, E.J., Lang, P.M., Masarie, K.A., Crotwell, A.M., Crotwell, M.J., 2015. Atmospheric Carbon Dioxide Dry Air Mole Fractions from the NOAA ESRL Carbon Cycle Cooperative Global Air Sampling Network, 1968–2014, Version: 2015-08-03. ftp://aftp.cmdl.noaa.gov/data/trace_gases/co2/flask/surface/.
- Frankignoulle, M., Borges, A.V., 2001. European continental shelf as a significant sink for atmospheric carbon dioxide. *Global Biogeochem. Cy.* 15, 569–576. doi:10.1029/2000GB001307
- Fritsch, F., Carlson, R., 1980. Monotone piecewise cubic interpolation. *SIAM J. Numer. Anal.* 17, 238–246. doi:10.1137/0717021
- García-Martín, E.E., Daniels, C.J., Davidson, K., Lozano, J., Mayers, K.M.J., McNeill, S., Mitchell, E., Poulton, A.J., Purdie, D.A., Tarran, G.A., Whyte, C., Robinson, C., 2017. Plankton community respiration and bacterial metabolism in a North Atlantic Shelf Sea during spring bloom development (April 2015). *Prog. Oceanogr.* doi:10.1016/j.pocean.2017.11.002
- Gowen, R.J., Hydes, D.J., Mills, D.K., Stewart, B.M., Brown, J., Gibson, C.E., Shammon, T.M., Allen, M., Malcolm, S.J., 2002. Assessing Trends in Nutrient Concentrations in

- Coastal Shelf Seas: a Case Study in the Irish Sea. *Estuar. Coast. Shelf S.* 54, 927–939. doi:10.1006/ecss.2001.0849
- Hartman, S., Humphreys, M., Kivimäe, C., Woodward, M., Kitidis, V., McGrath, T., Hydes, D., Greenwood, N., Ostle, C., Pearce, D., Sivy, D., Stewart, B., Walsham, P., McGovern, E., Harris, C., Griffiths, A., Smilenova, A., Clarke, J., Davis, C., Nightingale, P., 2017. Seasonality and spatial heterogeneity of the surface water carbonate system on the NW European shelf. *Prog. Oceanogr.* in press.
- Hopkinson, C.S., Fry, B., Nolin, A.L., 1997. Stoichiometry of dissolved organic matter dynamics on the continental shelf of the northeastern U.S.A. *Cont. Shelf Res.* 17, 473–489. doi:10.1016/S0278-4343(96)00046-5
- Humphreys, M.P., 2015a. Calculating seawater total alkalinity from open-cell titration data using a modified Gran plot technique, in: *Measurements and Concepts in Marine Carbonate Chemistry*. PhD Thesis, Ocean and Earth Science, University of Southampton, UK, pp. 25–44.
- Humphreys, M.P., 2015b. Cross-over analysis of hydrographic variables: XOVER v1.0. Ocean and Earth Science, University of Southampton, UK pp 8. doi:10.13140/RG.2.1.1629.0405
- Hydes, D.J., Gowen, R.J., Holliday, N.P., Shammon, T., Mills, D., 2004. External and internal control of winter concentrations of nutrients (N, P and Si) in north-west European shelf seas. *Estuar. Coast. Shelf S.* 59, 151–161. doi:10.1016/j.ecss.2003.08.004
- IPCC, 2013. *Climate Change 2013: The Physical Science Basis. Contribution of Working Group I to the Fifth Assessment Report of the Intergovernmental Panel on Climate Change*. Cambridge University Press, Cambridge, United Kingdom and New York, NY, USA.
- Ivanov, V.V., Shapiro, G.I., Huthnance, J.M., Aleynik, D.L., Golovin, P.N., 2004. Cascades of dense water around the world ocean. *Prog. Oceanogr.* 60, 47–98. doi:10.1016/j.pocean.2003.12.002
- Johnson, M.T., Greenwood, N., Sivy, D.B., Thomson, M., Reeve, A., Weston, K., Jickells, T.D., 2013. Characterising the seasonal cycle of dissolved organic nitrogen using Cefas SmartBuoy high-resolution time-series samples from the southern North Sea. *Biogeochemistry* 113, 23–36. doi:10.1007/s10533-012-9738-8
- Jones, D.C., Ito, T., Takano, Y., Hsu, W.-C., 2014. Spatial and seasonal variability of the air-sea equilibration timescale of carbon dioxide. *Global Biogeochem. Cy.* 28, 1163–1178. doi:10.1002/2014GB004813
- Kahaner, D., Moler, C., Nash, S., 1988. *Numerical Methods and Software*. Prentice Hall, Englewood Cliffs, NJ, U.S.A.
- Kitidis, V., Tait, K., Nunes, J., Brown, I., Woodward, E.M.S., Harris, C., Sabadel, A.J.M., Sivy, D.B., Silburn, B., Kröger, S., 2017. Seasonal benthic nitrogen cycling in a temperate shelf sea: the Celtic Sea. *Biogeochemistry* 1–17. doi:10.1007/s10533-017-0311-3
- Laruelle, G.G., Lauerwald, R., Pfeil, B., Regnier, P., 2014. Regionalized global budget of the CO₂ exchange at the air-water interface in continental shelf seas. *Global Biogeochem. Cy.* 28, 2014GB004832. doi:10.1002/2014GB004832
- Lawrence, M.G., 2005. The Relationship between Relative Humidity and the Dewpoint Temperature in Moist Air: A Simple Conversion and Applications. *Bull. Amer. Meteor. Soc.* 86, 225–233. doi:10.1175/BAMS-86-2-225
- Le Menn, M., 2011. About uncertainties in practical salinity calculations. *Ocean Sci.* 7, 651–659. doi:10.5194/os-7-651-2011

- Le Quéré, C., Raupach, M.R., Canadell, J.G., Marland, G., Bopp, L., Ciais, P., Conway, T.J., Doney, S.C., Feely, R.A., Foster, P., Friedlingstein, P., Gurney, K., Houghton, R.A., House, J.I., Huntingford, C., Levy, P.E., Lomas, M.R., Majkut, J., Metzl, N., Ometto, J.P., Peters, G.P., Prentice, I.C., Randerson, J.T., Running, S.W., Sarmiento, J.L., Schuster, U., Sitch, S., Takahashi, T., Viovy, N., van der Werf, G.R., Woodward, F.I., 2009. Trends in the sources and sinks of carbon dioxide. *Nature Geosci.* 2, 831–836. doi:10.1038/ngeo689
- Lee, K., Kim, T.-W., Byrne, R.H., Millero, F.J., Feely, R.A., Liu, Y.-M., 2010. The universal ratio of boron to chlorinity for the North Pacific and North Atlantic oceans. *Geochim. Cosmochim. Acta* 74, 1801–1811. doi:10.1016/j.gca.2009.12.027
- Lueker, T.J., Dickson, A.G., Keeling, C.D., 2000. Ocean $p\text{CO}_2$ calculated from dissolved inorganic carbon, alkalinity, and equations for K_1 and K_2 : validation based on laboratory measurements of CO_2 in gas and seawater at equilibrium. *Mar. Chem.* 70, 105–119. doi:10.1016/S0304-4203(00)00022-0
- Marrec, P., Cariou, T., Macé, E., Morin, P., Salt, L.A., Vernet, M., Taylor, B., Paxman, K., Bozec, Y., 2015. Dynamics of air–sea CO_2 fluxes in the northwestern European shelf based on voluntary observing ship and satellite observations. *Biogeosciences* 12, 5371–5391. doi:10.5194/bg-12-5371-2015
- McDougall, T.J., Barker, P.M., 2011. Getting started with TEOS-10 and the Gibbs Seawater (GSW) Oceanographic Toolbox. SCOR/IAPSO WG127.
- McGrath, T., McGovern, E., Cave, R.R., Kivimäe, C., 2015. The Inorganic Carbon Chemistry in Coastal and Shelf Waters Around Ireland. *Estuar. Coast.* 1–13. doi:10.1007/s12237-015-9950-6
- Olsen, A., Key, R.M., Heuven, S. van, Lauvset, S.K., Velo, A., Lin, X., Schirnick, C., Kozyr, A., Tanhua, T., Hoppema, M., Jutterström, S., Steinfeldt, R., Jeansson, E., Ishii, M., Pérez, F.F., Suzuki, T., 2016. The Global Ocean Data Analysis Project version 2 (GLODAPv2) – an internally consistent data product for the world ocean. *Earth Syst. Sci. Data* 8, 297–323. doi:10.5194/essd-8-297-2016
- Pingree, R.D., Holligan, P.M., Mardell, G.T., Head, R.N., 1976. The influence of physical instability on spring, summer and autumn phytoplankton blooms in the Celtic Sea. *J. Mar. Biol. Assoc. U.K.* 56, 845–873. doi:10.1017/S0025315400020919
- Pingree, R.D., Le Cann, B., 1989. Celtic and Armorican slope and shelf residual currents. *Prog. Oceanogr.* 23, 303–338. doi:10.1016/0079-6611(89)90003-7
- Redfield, A.C., 1934. On the proportions of organic derivatives in sea water and their relation to the composition of plankton, in: James Johnstone Memorial Volume. University Press of Liverpool, pp. 176–192.
- Redfield, A.C., Ketchum, B.H., Richards, F.A., 1963. The influence of organisms on the composition of sea-water, in: *The Sea*. Interscience, New York, pp. 26–77.
- Ruiz-Castillo, E., Sharples, J., Hopkins, J.E., Woodward, E.M.S., 2017. Seasonality in the cross-shelf physical structure and the implications for nutrients supplies to a temperate shelf sea. *Prog. Oceanogr.* in review.
- Seguro, I., Marca, A.D., Painting, S.J., Shutler, J.D., Suggett, D.J., Kaiser, J., 2017. High-resolution net and gross biological production during a Celtic Sea spring bloom. *Prog. Oceanogr.* doi:10.1016/j.pocean.2017.12.003
- Shapiro, G.I., Huthnance, J.M., Ivanov, V.V., 2003. Dense water cascading off the continental shelf. *J. Geophys. Res.* 108, 3390. doi:10.1029/2002JC001610
- Suykens, K., Delille, B., Chou, L., De Bodt, C., Harlay, J., Borges, A.V., 2010. Dissolved inorganic carbon dynamics and air-sea carbon dioxide fluxes during coccolithophore blooms in the northwest European continental margin (northern Bay of Biscay). *Global Biogeochem. Cy.* 24, GB3022. doi:10.1029/2009GB003730

- Suykens, K., Schmidt, S., Delille, B., Harlay, J., Chou, L., De Bodt, C., Fagel, N., Borges, A.V., 2011. Benthic remineralization in the northwest European continental margin (northern Bay of Biscay). *Cont. Shelf Res.* 31, 644–658. doi:10.1016/j.csr.2010.12.017
- Takahashi, T., Broecker, W.S., Langer, S., 1985. Redfield Ratio Based on Chemical Data from Isopycnal Surfaces. *J. Geophys. Res.* 90, 6907–6924. doi:10.1029/JC090iC04p06907
- Takahashi, T., Sutherland, S.C., Wanninkhof, R., Sweeney, C., Feely, R.A., Chipman, D.W., Hales, B., Friederich, G., Chavez, F., Sabine, C., Watson, A., Bakker, D.C.E., Schuster, U., Metzl, N., Yoshikawa-Inoue, H., Ishii, M., Midorikawa, T., Nojiri, Y., Körtzinger, A., Steinhoff, T., Hoppema, M., Olafsson, J., Arnarson, T.S., Tilbrook, B., Johannessen, T., Olsen, A., Bellerby, R., Wong, C.S., Delille, B., Bates, N.R., de Baar, H.J.W., 2009. Climatological mean and decadal change in surface ocean $p\text{CO}_2$, and net sea–air CO_2 flux over the global oceans. *Deep-Sea Res. Pt II* 56, 554–577. doi:10.1016/j.dsr2.2008.12.009
- Thomas, H., Bozec, Y., Elkalay, K., Baar, H.J.W. de, 2004. Enhanced Open Ocean Storage of CO_2 from Shelf Sea Pumping. *Science* 304, 1005–1008. doi:10.1126/science.1095491
- Tsunogai, S., Watanabe, S., Sato, T., 1999. Is there a “continental shelf pump” for the absorption of atmospheric CO_2 ? *Tellus B* 51, 701–712. doi:10.1034/j.1600-0889.1999.t01-2-00010.x
- van Heuven, S., Pierrot, D., Rae, J.W.B., Lewis, E., Wallace, D.W.R., 2011. CO_2SYS v 1.1, MATLAB program developed for CO_2 system calculations. ORNL/CDIAC-105b. Carbon Dioxide Information Analysis Center, Oak Ridge National Laboratory, U.S. Department of Energy, Oak Ridge, TN, USA.
- Volk, T., Hoffert, M.I., 1985. Ocean Carbon Pumps: Analysis of Relative Strengths and Efficiencies in Ocean-Driven Atmospheric CO_2 Changes, in: Sundquist, E.T., Broecker, W.S. (Eds.), *The Carbon Cycle and Atmospheric CO_2 : Natural Variations Archean to Present*. American Geophysical Union, USA, pp. 99–110.
- Wakelin, S.L., Holt, J.T., Blackford, J.C., Allen, J.I., Butenschön, M., Artioli, Y., 2012. Modeling the carbon fluxes of the northwest European continental shelf: Validation and budgets. *J. Geophys. Res. Oceans* 117, C05020. doi:10.1029/2011JC007402
- Wanninkhof, R., 2014. Relationship between wind speed and gas exchange over the ocean revisited: Gas exchange and wind speed over the ocean. *Limnol. Oceanogr. Methods* 12, 351–362. doi:10.4319/lom.2014.12.351
- Weiss, R.F., 1974. Carbon dioxide in water and seawater: the solubility of a non-ideal gas. *Mar. Chem.* 2, 203–215. doi:10.1016/0304-4203(74)90015-2
- Wihsgott, J., Hopkins, J., Sharples, J., Jones, E., Balfour, C.A., 2016. Long-term mooring observations of full depth water column structure spanning 17 months, collected in a temperate shelf sea (Celtic Sea). British Oceanographic Data Centre, Natural Environment Research Council, UK. doi:10/bqwf
- Wihsgott, J.U., Sharples, J., Hopkins, J.E., Woodward, E.M.S., Greenwood, N., Hull, T., Sivy, D.B., 2017. Investigating the autumn bloom’s significance within the seasonal cycle of primary production in a temperate shelf sea. *Prog. Oceanogr.* in review.
- Wollast, R., 1998. Evaluation and comparison of the global carbon cycle in the coastal zone and in the open ocean, in: Brink, K. H., Robinson, A. R. (Eds.), *The Global Coastal Ocean*. John Wiley and Sons, New York, pp. 213–252.
- Woodward, E.M.S., Rees, A.P., 2001. Nutrient distributions in an anticyclonic eddy in the northeast Atlantic Ocean, with reference to nanomolar ammonium concentrations. *Deep-Sea Res. Pt II* 48, 775–793. doi:10.1016/S0967-0645(00)00097-7

937 **7. Tables**

938 Table 1. Summary of the time intervals used in the CCS site analysis.

Name of time interval	Year	Interval code	Sampling date range (dd/mm/yyyy)	Cruise(s)
Winter	2014	W14	26/03/2014 – 27/03/2014	DY008
Late Spring	2014	lSp14	19/06/2014 – 22/06/2014	JC105
Summer	2014	Su14	05/08/2014 – 23/08/2014	DY026A, DY026B
Autumn	2014	A14	10/11/2014 – 29/11/2014	DY018
Winter	2015	W14	22/03/2015	DY021
In-bloom 1	2015	IB1	03/04/2015 – 06/04/2015	DY029
In-bloom 2	2015	IB2	11/04/2015 – 12/04/2015	DY029
In-bloom 3	2015	IB3	15/04/2015	DY029
In-bloom 4	2015	IB4	16/04/2015	DY029
In-bloom 5	2015	IB5	20/04/2015	DY029
In-bloom 6	2015	IB6	21/04/2015	DY029
In-bloom 7	2015	IB7	25/04/2015 – 26/04/2015	DY029
In-bloom 8	2015	IB8	28/04/2015	DY029
Early Spring	2015	eSp15	21/05/2015 – 23/05/2015	DY030
Summer	2015	Su15	24/07/2015 – 23/08/2015	DY033, DY034

939

940

941 Table 2. Details of the empirical algorithm used to predict surface $p\text{CO}_2^{\text{sw}}$ at CCS.

Day of year (DoY) range	SST range / °C	$p\text{CO}_2^{\text{sw}}$ / μatm
$80 < \text{DoY} < 232$	$\text{SST} < 10.5$	$1.547 \times 10^{-3} \exp(\text{SST}) + 372.7$
$80 < \text{DoY} < 232$	$10.5 \leq \text{SST} \leq 11.0$	$324.5 + 6.596 \times 10^{24} \exp[-5.000(\text{SST})]$
$80 < \text{DoY} < 232$	$11.0 < \text{SST}$	$-0.557(\text{SST})^2 + 23.57(\text{SST}) + 141.1$
$\text{DoY} \leq 80$ or $233 \leq \text{DoY}$	All	$-0.2479(\text{SST})^3 + 10.846(\text{SST})^2 - 151.42(\text{SST}) + 1050.3$

942

943

944

945

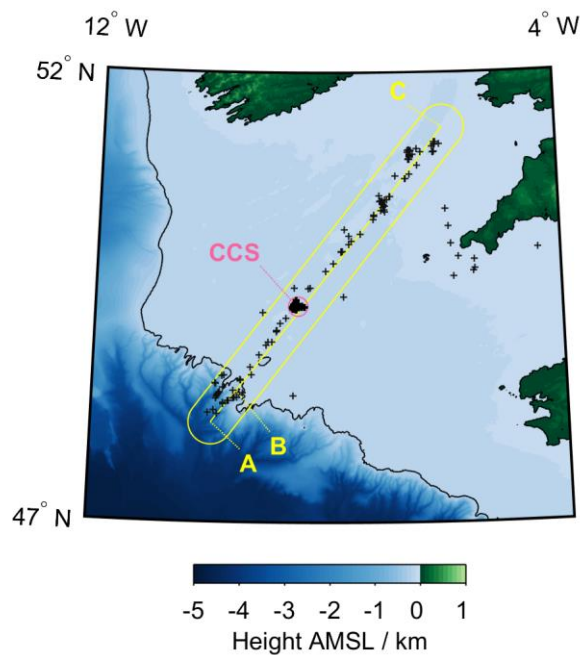
946 Table 3. Correlation statistics between biogeochemical variables and salinity. Columns headed dX/dS contain gradient \pm its standard error in
 947 $\mu\text{mol kg}^{-1}$ (Figure 8); N is the number of observations used in each regression.

Cruise	Interval code	C_T				DIN				SRP			
		dC_T/dS	r^2	p	N	$dDIN/dS$	r^2	p	N	$dSRP/dS$	r^2	p	N
DY008	W14	-10.6 ± 8.9	0.11	0.26	13	7.6 ± 0.6	0.86	0.00	25	-0.23 ± 0.09	0.21	0.02	25
JC105	lSp14	-109.6 ± 10.0	0.86	0.00	21	1.0 ± 0.8	0.07	0.24	21	-0.46 ± 0.06	0.75	0.00	21
DY026*	Su14	-60.6 ± 10.8	0.78	0.00	11	4.1 ± 1.2	0.36	0.00	23	-0.29 ± 0.06	0.47	0.00	26
DY018	A14	-99.5 ± 10.6	0.49	0.00	92	-0.2 ± 1.1	0.00	0.89	183	-0.46 ± 0.07	0.18	0.00	202
DY021	W15	-19.6 ± 9.1	0.28	0.05	14	5.9 ± 0.7	0.59	0.00	47	0.01 ± 0.06	0.00	0.87	47
DY029	IB1–IB8	-39.5 ± 7.3	0.54	0.00	27	7.4 ± 0.4	0.65	0.00	192	0.11 ± 0.02	0.12	0.00	202
DY030	eS15	-26.7 ± 13.4	0.50	0.12	6	9.5 ± 1.2	0.85	0.00	13	0.32 ± 0.10	0.48	0.01	13
DY033	Su15	-63.1 ± 8.1	0.68	0.00	31	4.2 ± 0.4	0.42	0.00	182	-0.21 ± 0.02	0.30	0.00	186
DY034	Su15	-120.9 ± 24.0	0.78	0.00	9	0.4 ± 1.8	0.00	0.84	44	-0.51 ± 0.12	0.31	0.00	44

948 *DY026 includes all data from both DY026A and DY026B.

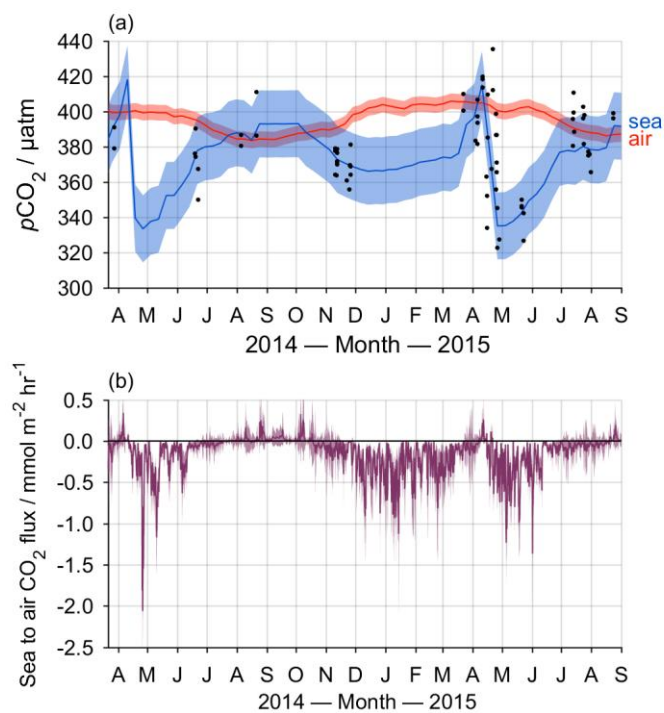
949

8. Figures



951

952 Figure 1. The UK-SSB sampling locations in the Celtic Sea. The pink circle contains the data
 953 considered to represent the Central Celtic Sea site (i.e. within 12 km of 49.4°N, 8.54°W),
 954 while the yellow lines indicate the transect route for Fig. 7 and enclose the data included in
 955 those plots; the points labelled A, B and C correspond to the equivalent points on Fig. 7. The
 956 200 m bathymetry contour, traditionally used to define the edge of the shelf, is shown as a
 957 black line. Topography data are from the GEBCO_2014 30 arc-second grid (version
 958 20150318, <http://www.gebco.net>).

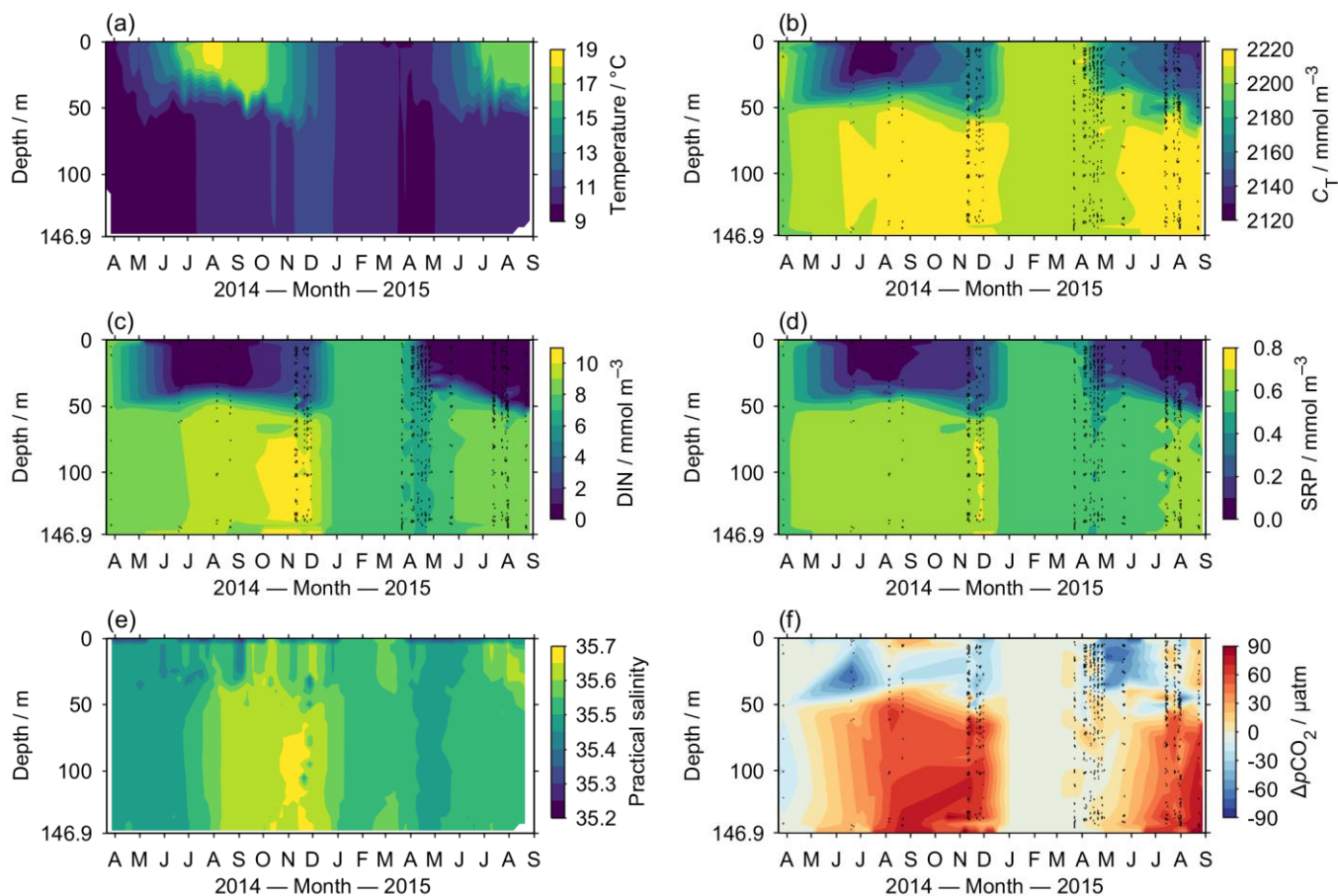


959

960 Figure 2. Time-series of air-sea CO_2 disequilibrium and flux at CCS. (a) Atmospheric (red)
 961 and sea surface (blue) $p\text{CO}_2$ at CCS. The black points show the actual measurements of
 962 surface $p\text{CO}_2^{\text{sw}}$, while the blue line shows our algorithm-predicted interpolation of these data
 963 (Table 2) that was used to calculate $\Delta p\text{CO}_2$ and then the air-sea CO_2 flux. (b) The sea to air
 964 CO_2 flux. The shaded areas show the 95% confidence intervals.

965

966



978 Figure 3. Hovmöller diagrams of CCS water column (a) temperature, (b) dissolved inorganic
 979 carbon, (c) dissolved inorganic nitrogen (i.e. nitrate + nitrate + ammonium), (d) soluble
 980 reactive phosphorus, (e) practical salinity, and (f) air-sea CO₂ disequilibrium. Where shown,
 981 sampling locations are indicated as black points. The cycle of winter mixing and summer
 982 stratification is clear for most variables, while S, DIN and SRP show an anomalous increase
 983 in the deep layer during late 2014, indicating an influx of open ocean waters.

984

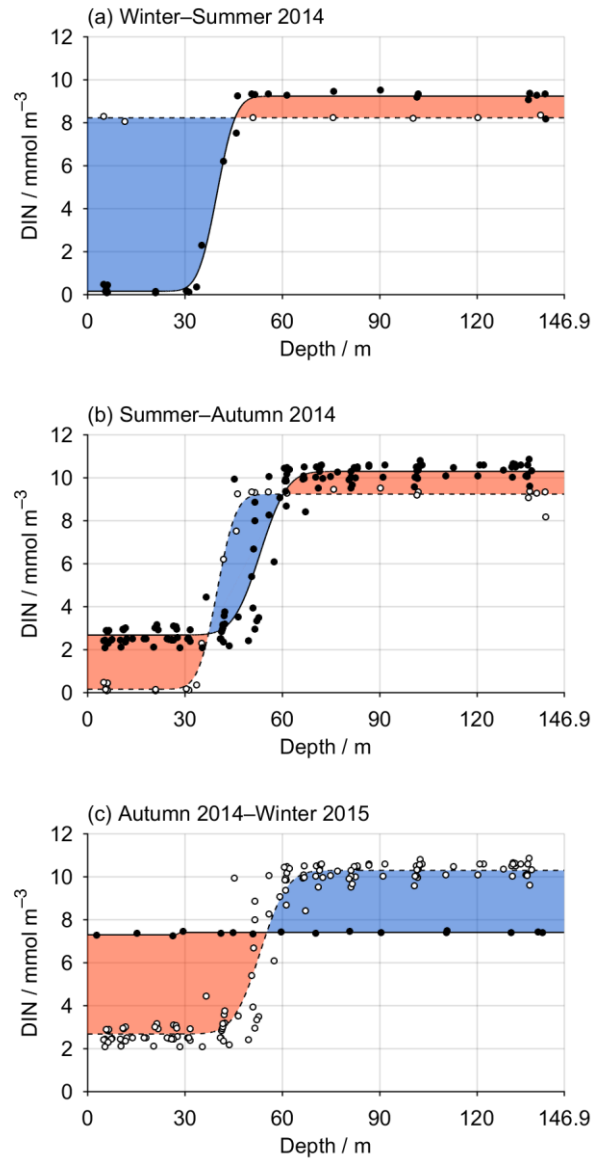


Figure 4. Changes in the DIN profile at CCS for selected time intervals. In each panel, the earlier profile is shown as a dashed line, while the later one is solid. The blue shaded areas therefore indicate decreases in DIN, while orange shows increases. (a) Primary production in the surface layer drew down DIN, while remineralisation at depth increased the DIN concentration. (b) The onset of vertical mixing eroded the surface-deep DIN gradient, overlaid by a remineralisation-driven increase in the total DIN inventory. (c) The water column returned to a vertically homogeneous state following further vertical mixing.

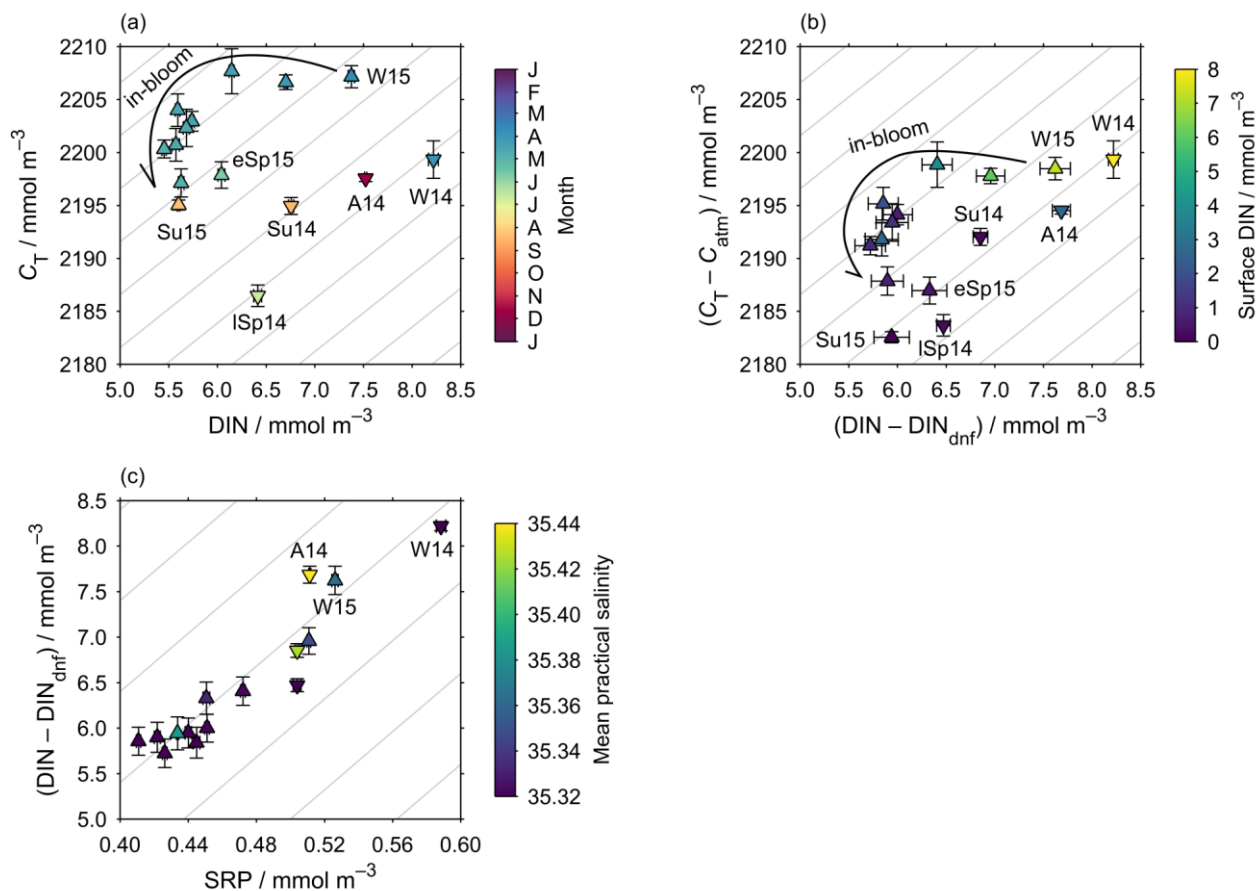


Figure 5. Water column inventories at CCS throughout the SSB study period. The inventories have been divided by the water depth, so the values shown are the vertical mean at each time point. Downwards/upwards pointing triangles represent 2014/2015 data respectively, and the grey diagonal lines indicate a C:N:P stoichiometry of 117:16:1 (Anderson and Sarmiento, 1994). W = winter; eSp = early spring; ISp = late spring; Su = summer; A = autumn; 14/15 indicates the year. (a) Raw inventories of C_T and N_T measured at CCS, coloured by the sampling date. (b) Here, the C_T inventory is corrected for air-sea gas exchange relative to the first sampling point, while the DIN is corrected for denitrification/anammox. The colour shows the surface layer DIN concentration. (c) Relative changes in DIN (corrected for denitrification/anammox) and SRP, coloured by mean salinity at CCS at each time point. Higher salinity values indicate the influence of open ocean waters.

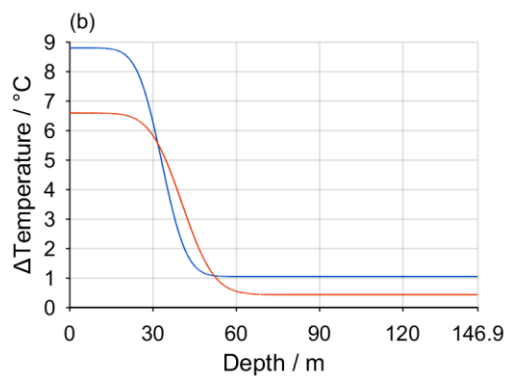
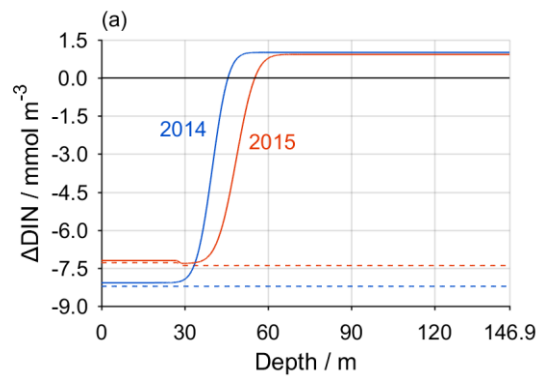


Figure 6. Winter to summer changes in (a) DIN and (b) seawater temperature for 2014 (blue) and 2015 (red). In (a), the dashed lines show the lowest possible ΔDIN , i.e. its value if the entire winter DIN inventory had been converted into OM. All available DIN in the surface layer was converted to OM in both years. This represented a greater change in DIN in 2014 due to the higher initial DIN concentration, but the deeper nutricline in 2015 led to greater NCP overall. Remineralisation increased the deep layer DIN concentration by the same amount in both years, but this represented a smaller absolute DIN addition in 2015 owing to the deeper nutricline.

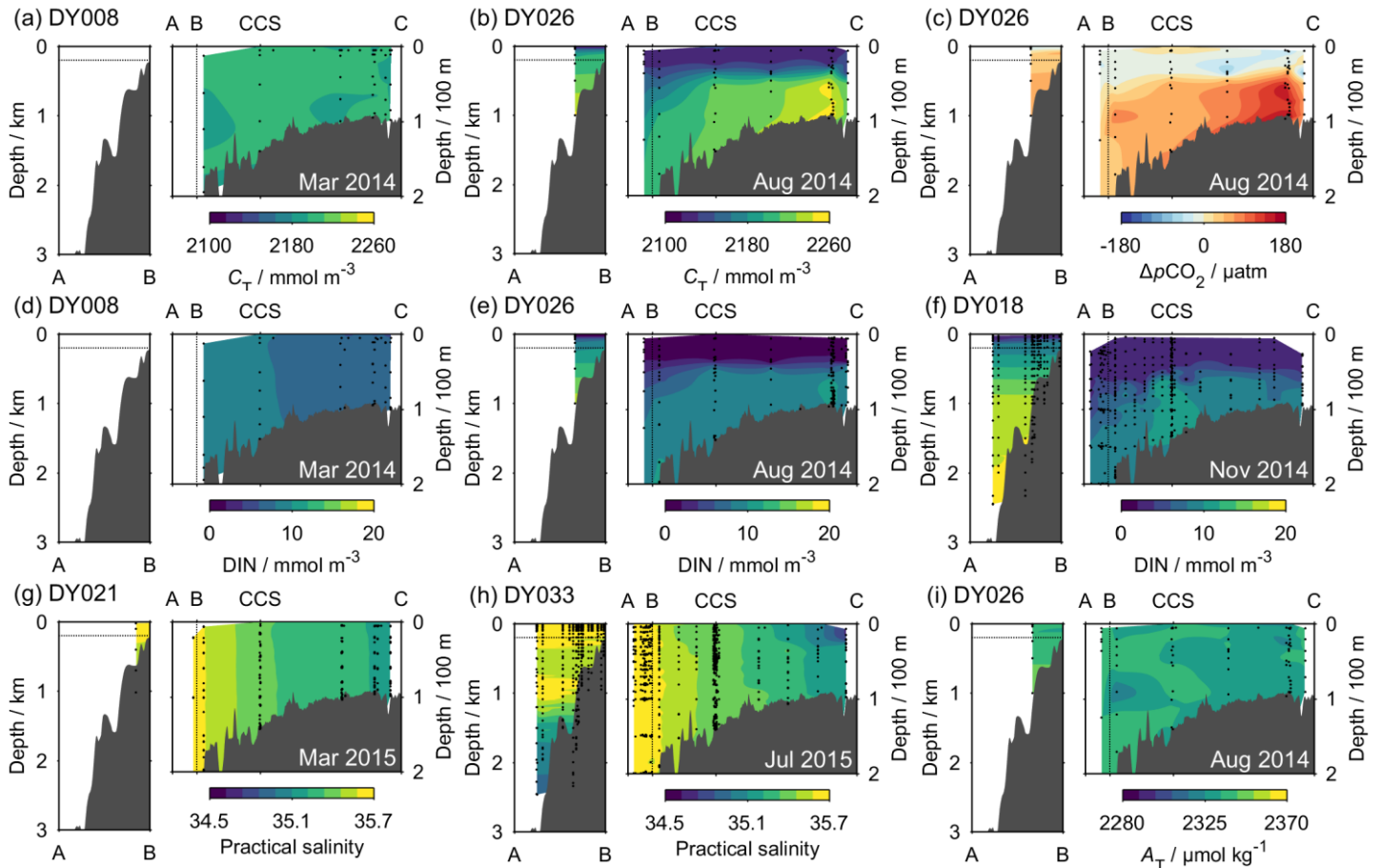


Figure 7. Transects across the Celtic Sea for selected variables and UK-SSB cruises. In each panel, the area above the horizontal dotted line in the left plot (shelf break) is the same as that to the left of the vertical dotted line in the right plot (on the shelf), and the black points indicate where samples were collected. Points A, B, CCS and C are located on Fig. 1. (a) and (b) show C_T in winter and summer 2014 respectively, while (c) shows ΔpCO_2 in summer 2014. (d), (e) and (f) show the evolution of DIN from spring through summer to autumn 2014. (g) and (h) illustrate changes in salinity between winter and summer 2015, while (i) shows A_T in summer 2014. A full set of transects for every variable and UK-SSB cruise is provided in Supp. Figs. S6–S11.

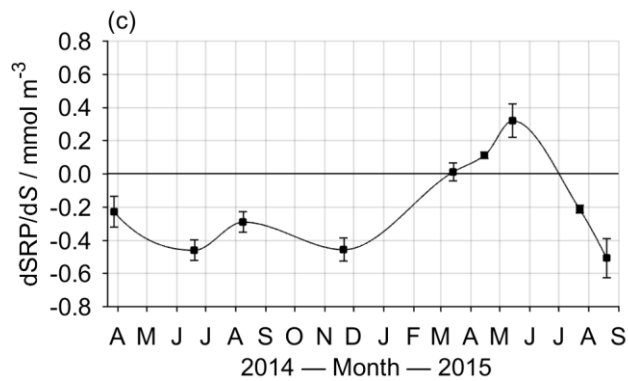
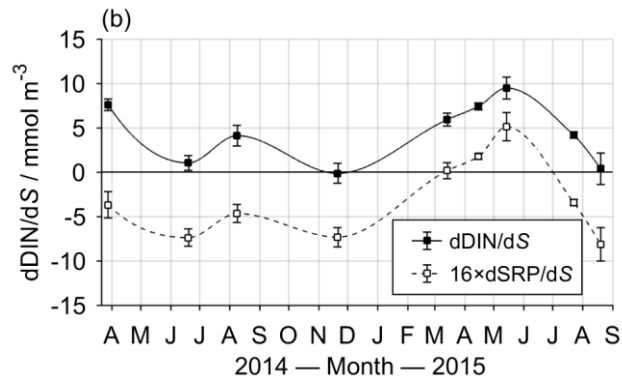
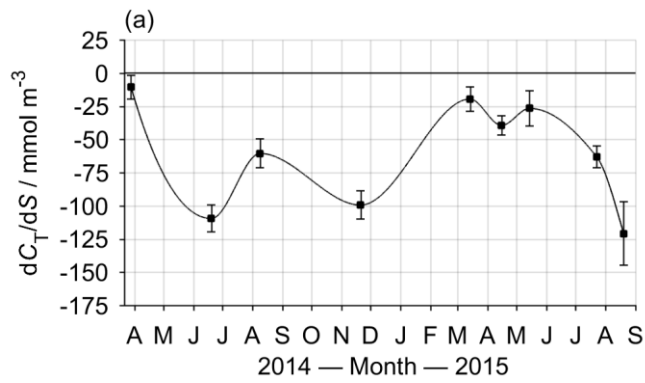
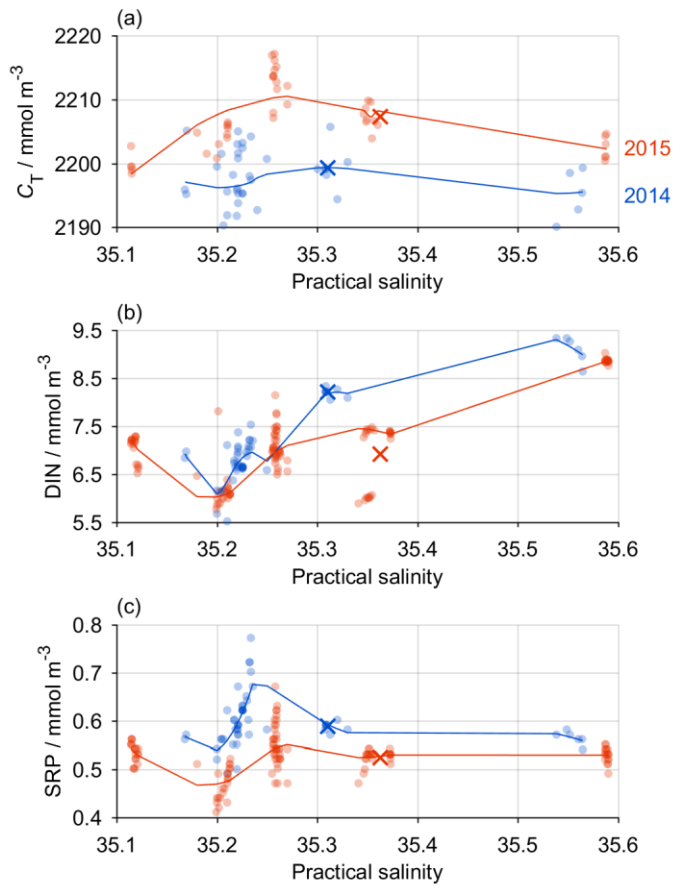


Figure 8. Time-series of regression slopes between S and (a) C_T , (b) DIN , and (c) SRP . Negative values indicate that the on-shelf deep layer is enriched in the nutrient relative to the open ocean, while positive values indicate on-shelf depletion. Error bars show the standard error in the gradient at each point (Table 3). In (b), the predicted relationship based on $dSRP/dS$ is also shown, considered to represent the component driven by OM remineralisation. The offset between this and the solid line (mean \pm SD difference = 7.5 ± 2.1 mmol m^{-3}) was likely driven by denitrification/anammox in the Celtic Sea; note that this offset value is reported per unit practical salinity (which is itself dimensionless).



1072

1073 Figure 9. Changes in (a) C_T , (b) DIN and (c) SRP, across the entire Celtic Sea transect from
 1074 winter 2014 (blue) to winter 2015 (red). The \times symbols show the mean conditions at CCS
 1075 each winter. Salinity values increase towards the open ocean. The increase in C_T observed at
 1076 CCS from winter 2014 to winter 2015, and corresponding declines in DIN and SRP, appear
 1077 to be consistent across much of the Celtic Sea, rather than being a feature of spatial
 1078 variability local to CCS.

1079

9. Supplementary information

9.1. Supplementary tables

Table S1. Summary of the UK-SSB research cruises.

Cruise code ^a	Cruise sampling dates (dd/mm/yy) ^b	Cruise Principle Investigator	C _T /A _T sample collectors	No. of C _T /A _T samples
DY008	21/03—04/04/14	H. A. Ruhl	L. Darroch	45
JC105	16/06—22/06/14	J. E. Hopkins	J. Fox, R. Houlding, P. Nelson	105
DY026A	04/08—13/08/14	R. Sanders	R. Sims	60
DY026B	17/08—22/08/14	D. Sivyer	R. Sims	16
DY018	10/11—01/12/14	J. Sharples	L. Darroch, J. E. Hopkins	301
DY021	03/03—24/03/15	E. M. S. Woodward	N. Hicks	47
DY029	02/04—28/04/15	A. Poulton	A. Poulton, K. Mayers	214
DY030	05/05—23/05/15	G. Fones	R. Sims	72
DY033	13/07—01/08/15	C. M. Moore	R. Sims	201
DY034	07/08—31/08/15	H. A. Ruhl		52

^aCruise codes beginning with DY were on the RRS *Discovery*, while JC stands for the RRS *James Cook*. ^bCruise sampling dates indicate the time period for collection of samples used in this study, not necessarily the entire duration of the cruises.

1088 Table S2. Coefficients fitted to Eq. (1) at CCS for each time interval (cf. Table 1 and Supp.
1089 Figs. S1–S4) for the variables DIC, DIN, DIP, and practical salinity. Units for v_0 and v_1 are
1090 the same as for the relevant variable (i.e. mmol m⁻³ for C_T , DIN and SRP, and dimensionless
1091 for practical salinity), while z_0 and z_1 are in m.

	C_T				DIN			
Interval code	v_0	v_1	z_0	z_1	v_0	v_1	z_0	z_1
W14	2199.3	0	0	0	8.22	0	0	0
lSp14	2168.9	38.70	40.0	9.64	4.64	4.391	43.8	6.80
Su14	2173.2	42.87	36.2	8.36	4.68	4.542	39.9	6.48
A14	2190.3	27.88	54.4	9.99	6.48	3.808	53.3	9.24
W15	2207.1	-1.08	80.0	12.38	7.34	0.056	28.0	0.69
IB1	2206.6	2.04	70.7	0.68	6.56	0.529	52.9	15.83
IB2	2203.6	7.86	35.8	13.93	5.37	1.465	34.3	17.85
IB3	2192.8	15.97	26.8	19.54	3.21	3.549	19.7	26.09
IB4	2197.8	12.38	36.5	15.30	4.37	2.385	35.8	18.15
IB5	2195.1	13.27	42.3	7.71	4.70	2.027	41.7	8.91
IB6	2195.5	11.54	30.2	13.78	4.06	2.897	32.4	8.04
IB7	2191.3	17.68	35.9	9.39	3.92	2.944	35.2	10.53
IB8	2186.6	21.58	37.7	3.21	4.03	3.247	37.2	4.89
eSp15	2186.4	21.92	35.1	4.04	4.17	3.634	35.6	5.34
Su15	2180.1	37.27	44.1	12.17	4.20	4.122	48.6	7.78
	SRP				Practical salinity			
Interval code	v_0	v_1	z_0	z_1	v_0	v_1	z_0	z_1
W14	0.59	0	0	0	35.310	0	0	0
lSp14	0.37	0.303	42.1	10.80	35.324	-0.0101	18.8	2.33
Su14	0.36	0.302	38.8	7.01	35.395	0.0429	21.8	17.17
A14	0.45	0.248	54.2	9.41	35.437	0.0444	58.1	2.45
W15	0.49	0.040	0.4	29.42	35.356	0.0096	15.0	3.33
IB1	0.50	0.025	51.6	12.65	35.343	0.0222	54.8	14.72
IB2	0.43	0.089	36.5	14.87	35.338	-0.0251	23.7	52.69
IB3	0.27	0.250	17.4	30.97	35.326	-0.0097	43.7	18.90
IB4	0.34	0.146	37.0	20.29	35.321	-0.0106	31.8	6.99
IB5	0.38	0.143	42.1	8.16	35.326	-0.0174	42.4	6.72

IB6	0.34	0.189	33.1	8.33	35.322	-0.0168	34.9	8.36
IB7	0.33	0.184	36.5	11.04	35.312	-0.0058	42.3	0.90
IB8	0.34	36.363	0.16	5.02	35.311	0.0041	35.3	2.01
eSp15	0.35	35.486	0.2	6.03	35.322	0.0218	35.9	7.20
Su15	0.34	48.082	0.27	9.08	35.398	-0.0266	35.1	0.03

1092

1093

9.2. Supplementary figures

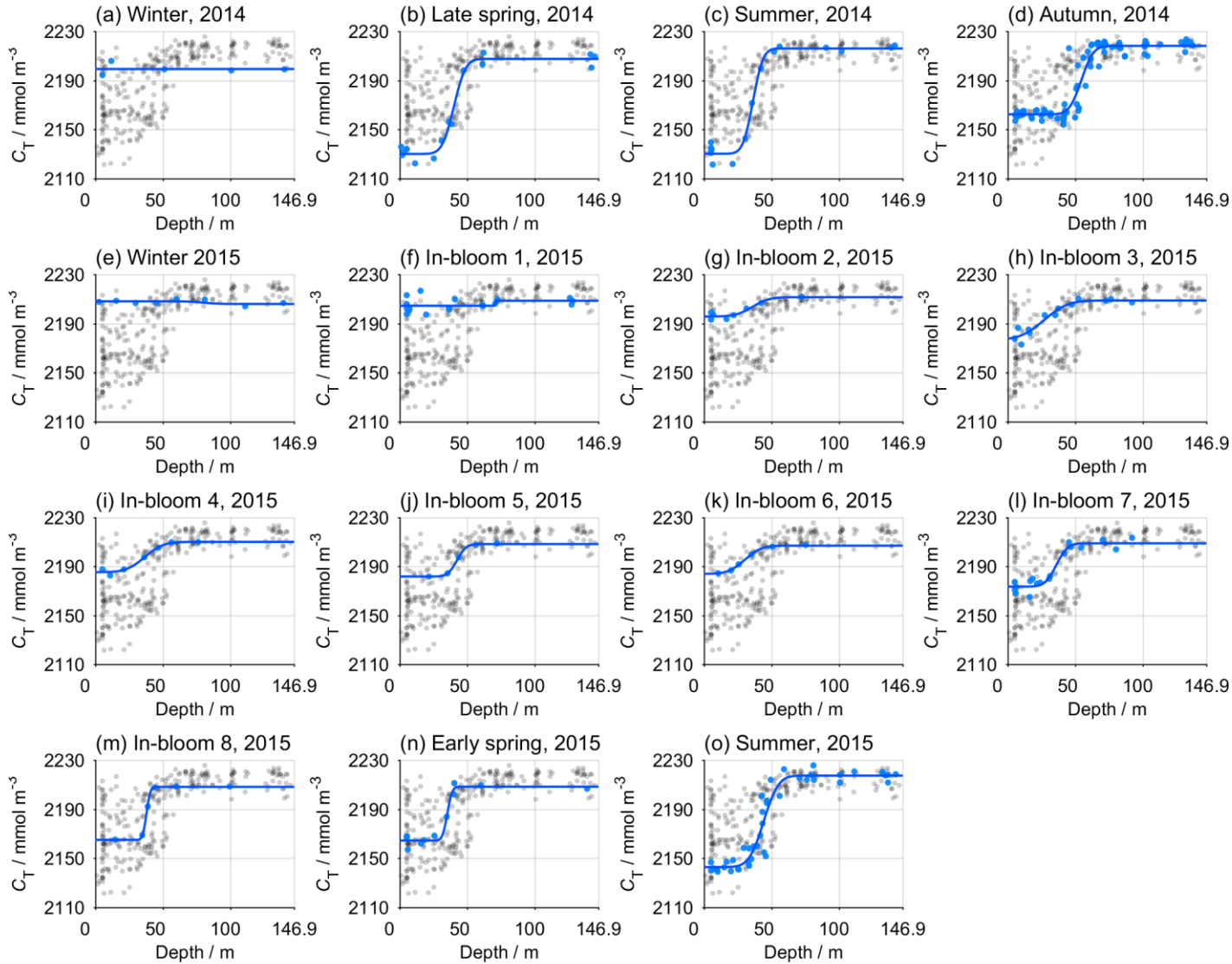
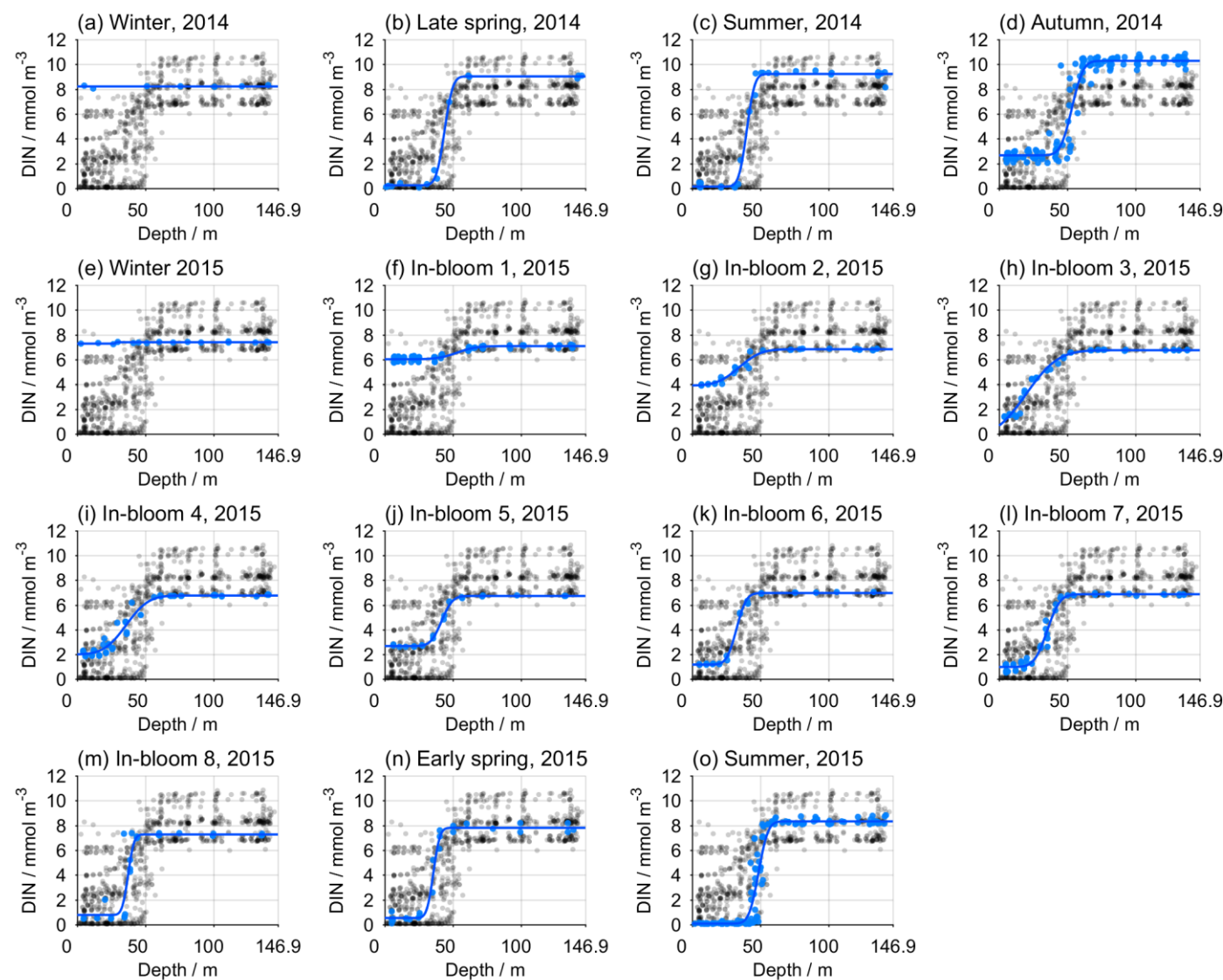


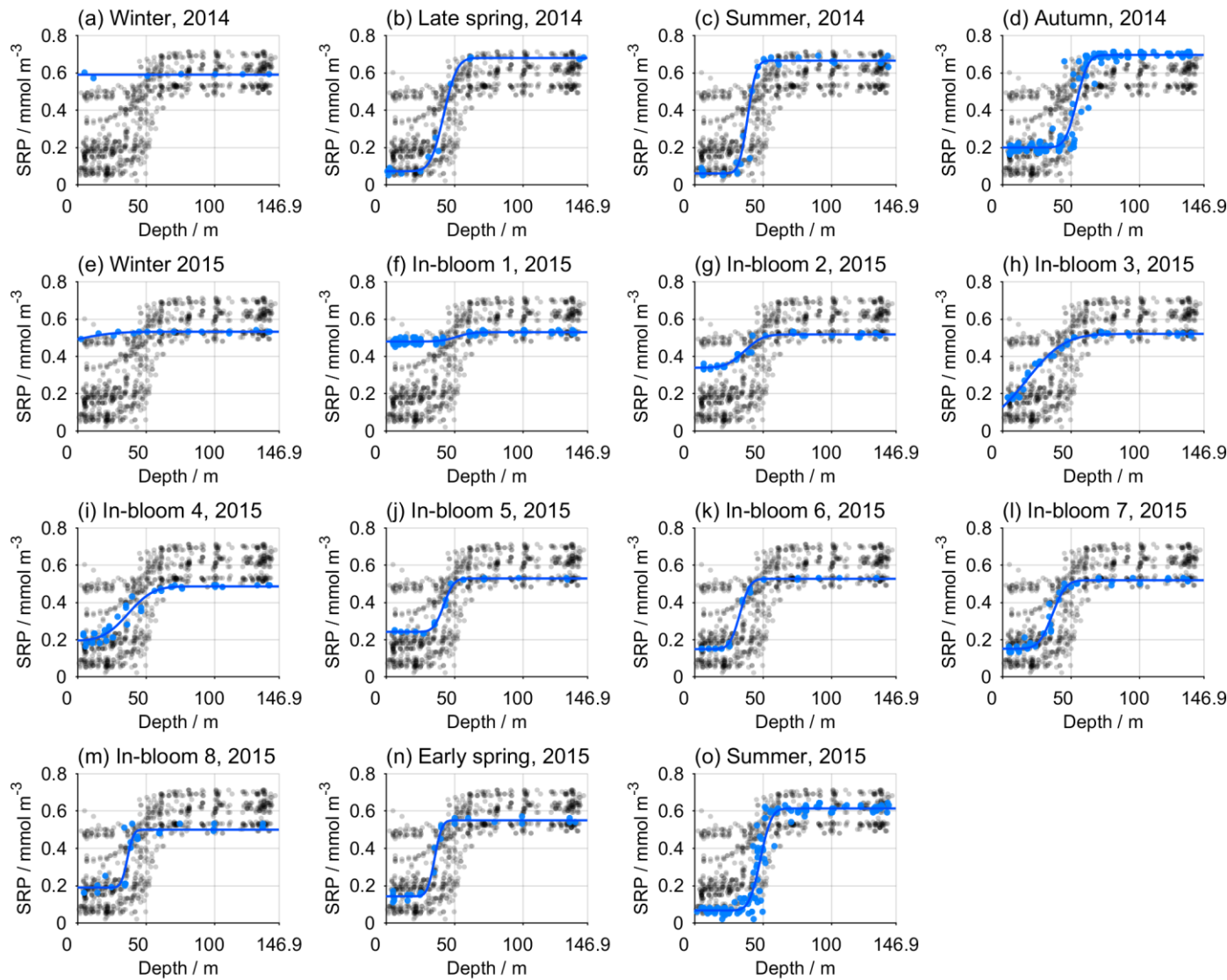
Figure S1. Dissolved inorganic carbon (C_T) profiles at each time point at CCS (Table 1). The grey circles show the entire CCS dataset, while the blue circles highlight the data at each time point. The blue line shows the final vertical profile used for inventory calculations (Supp. Table S2).

1116



1131 Figure S2. Dissolved inorganic nitrogen (DIN, nitrate + nitrite + ammonium) profiles at each
1132 time point at CCS (Table 1). The grey circles show the entire CCS dataset, while the blue
1133 circles show the data at each time point. The blue line shows the final vertical profile used for
1134 inventory calculations (Supp. Table S2).

1135



1151 Figure S3. Soluble reactive phosphorus (SRP) profiles at each time point at CCS (Table 1).
1152 The grey circles show the entire CCS dataset, while the blue circles show the data at each
1153 time point. The blue line shows the final vertical profile used for inventory calculations
1154 (Supp. Table S2).

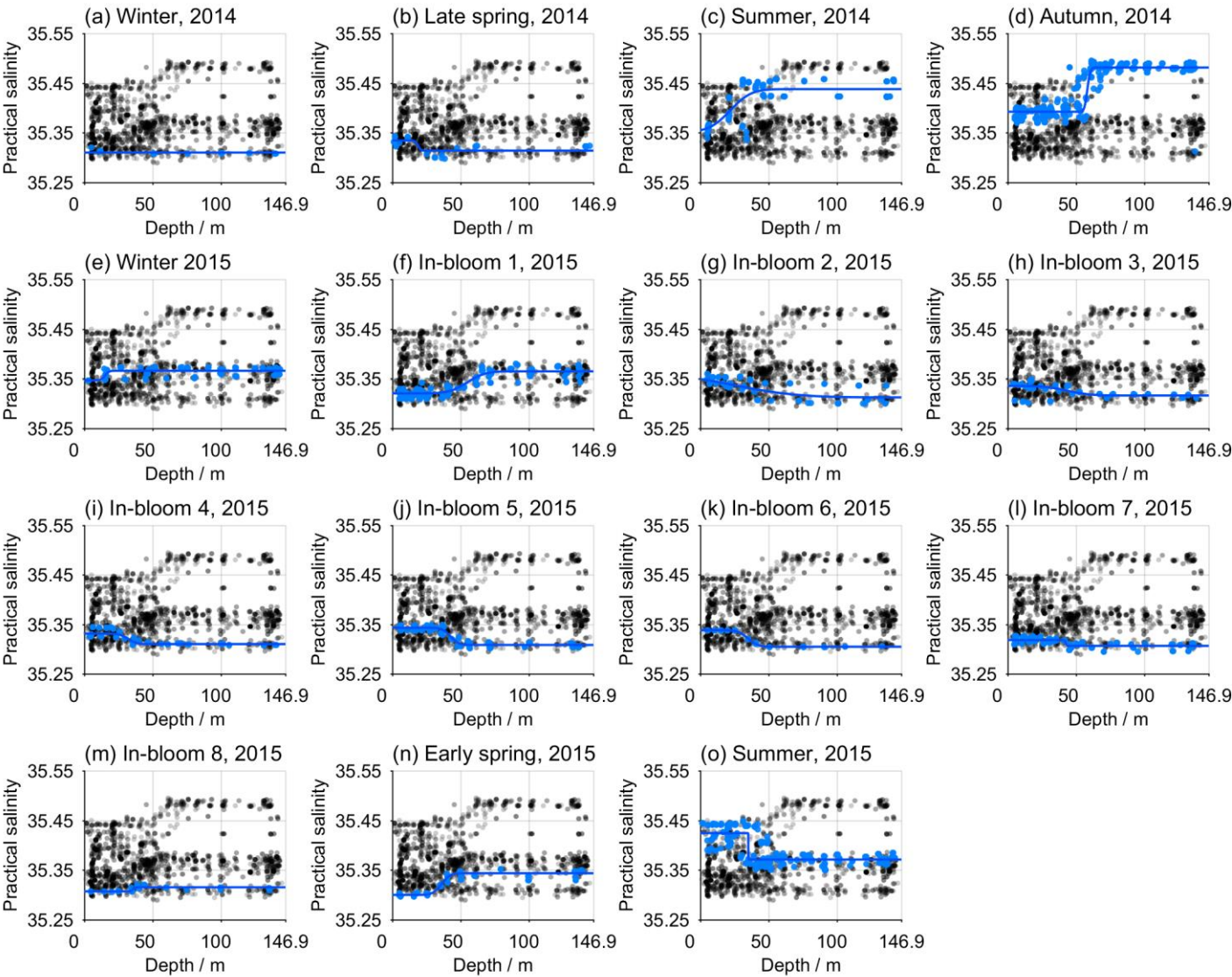
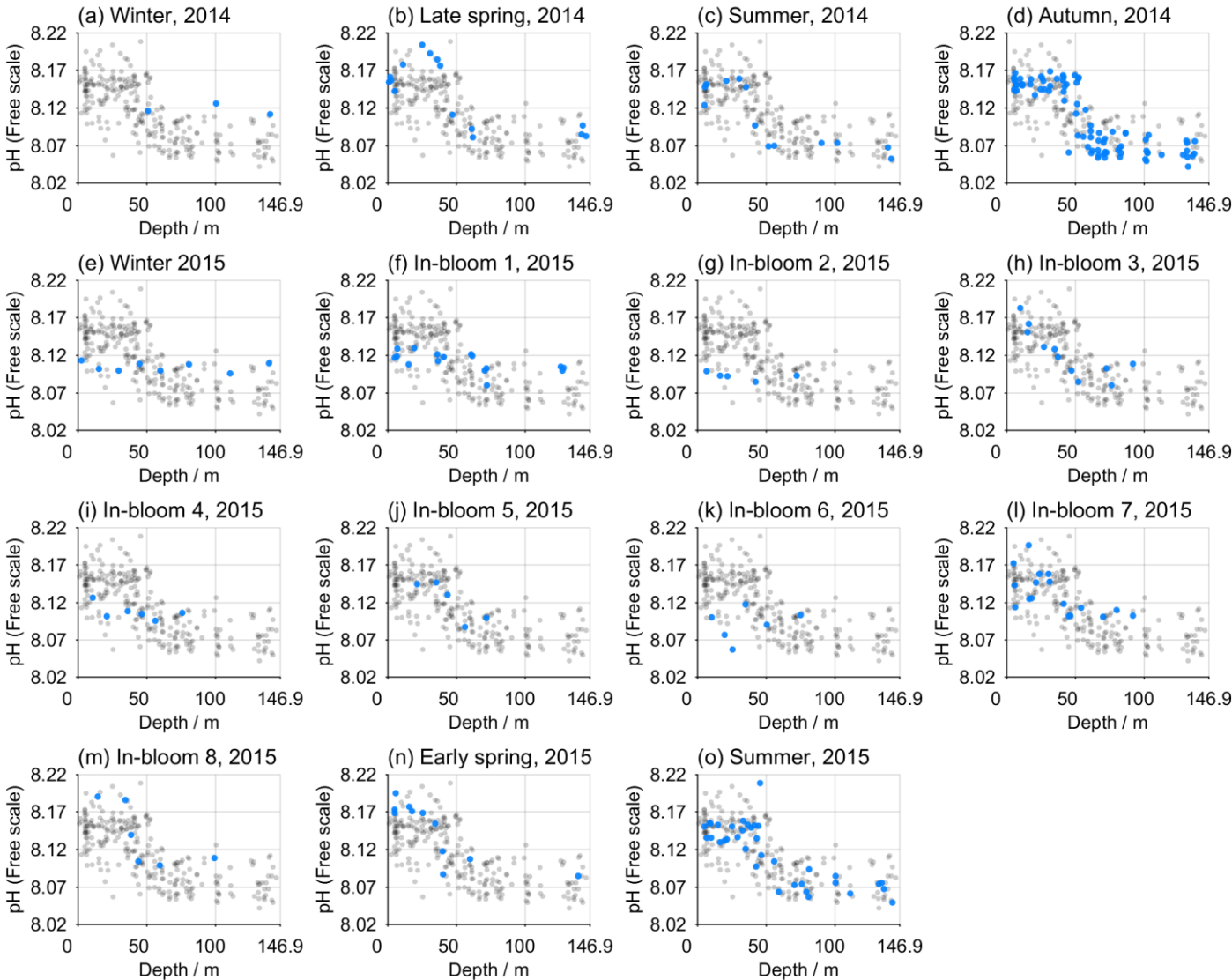


Figure S4. Practical salinity profiles at each time point at CCS (Table 1). The grey circles show the entire CCS dataset, while the blue circles show the data at each time point. The blue line shows the final vertical profile used for inventory calculations (Supp. Table S2).



1193 Figure S5. Seawater pH on the Free scale at each time point at CCS (Table 1), calculated
1194 from A_T and C_T measurements (van Heuven et al., 2011). The grey circles show the entire
1195 CCS dataset, while the blue circles show the data at each time point.

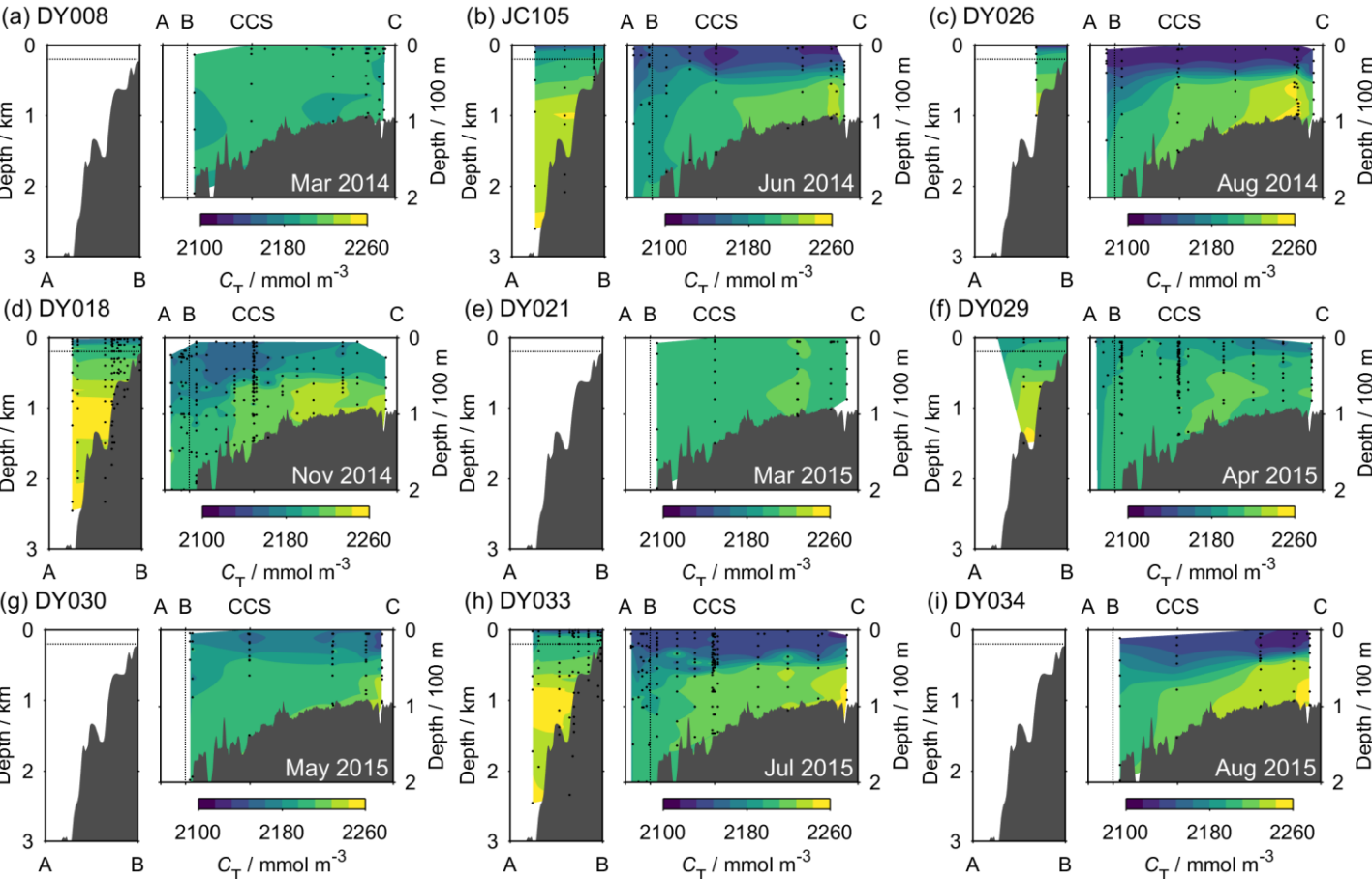
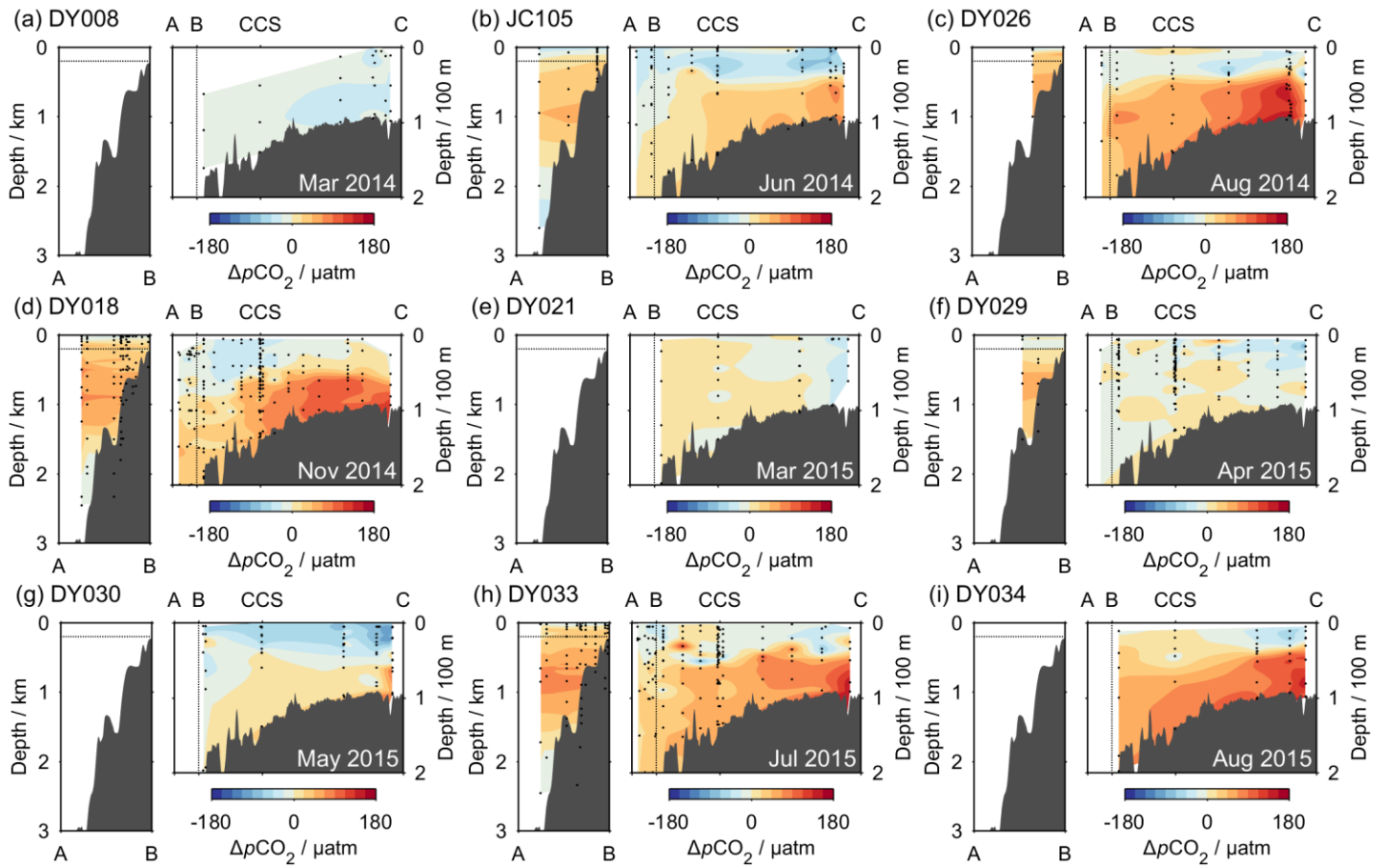


Figure S6. Transects of dissolved inorganic carbon (C_T) measured across the Celtic Sea for all of the SSB cruises. In each panel, the area above the horizontal dotted line in the left plot is the same as that to the left of the vertical dotted line in the right plot. Black points indicate the sample locations. The geographical locations of points A, B, CCS and C are shown by Fig. 1.

1215



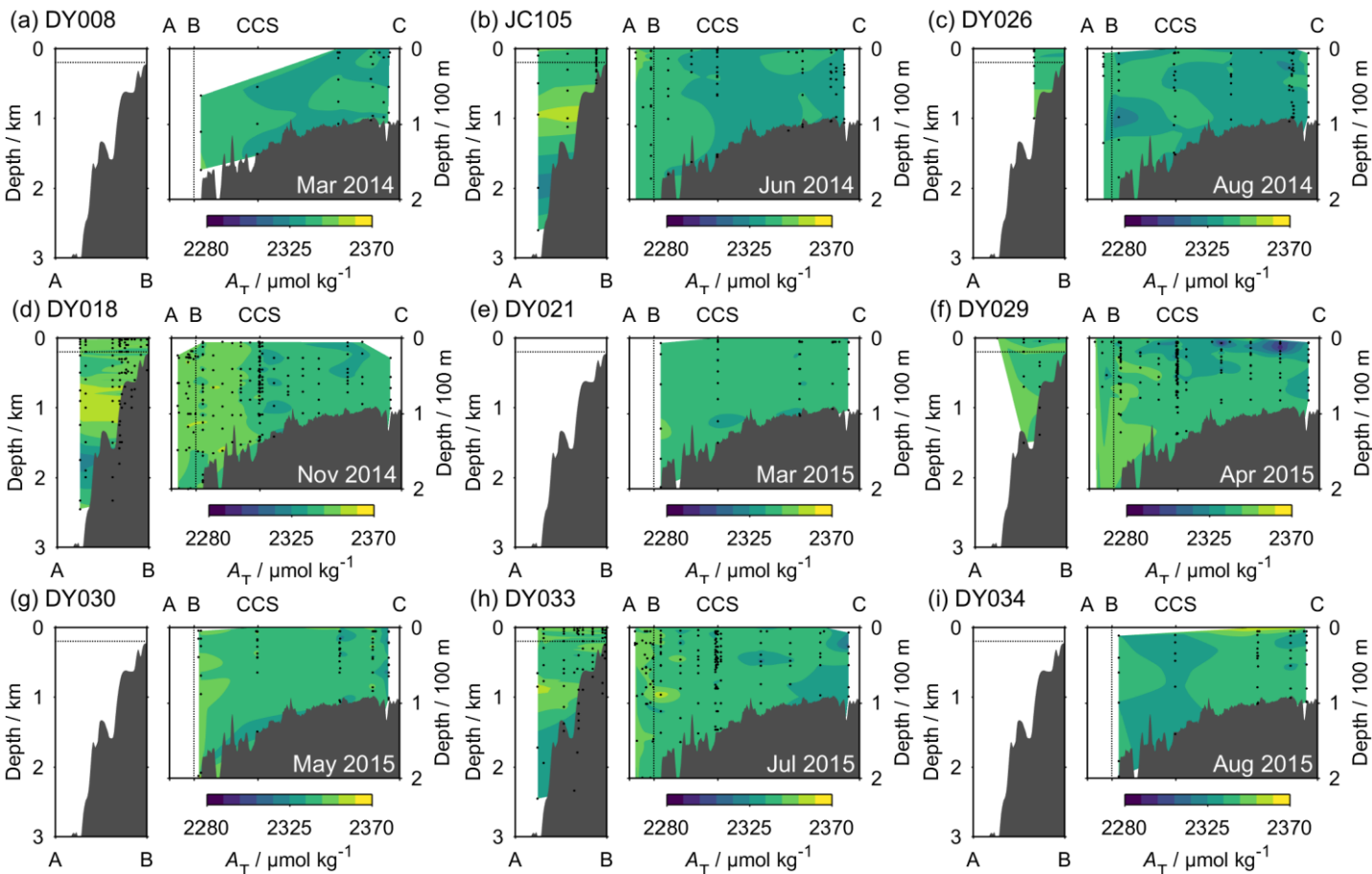
1227 Figure S7. Transects of $\Delta p\text{CO}_2$, calculated from C_T and A_T measurements, across the Celtic

1228 Sea for each SSB cruise. The layout is as described for Fig. 7.

1229

1230

1231



1243

1244

1245

1246

1247

1248

Figure S8. Transects of total alkalinity (A_T) across the Celtic Sea for all of the UK-SSB cruises. In each panel, the area above the horizontal dotted line in the left plot is the same as that to the left of the vertical dotted line in the right plot. Black circles indicate sample locations.

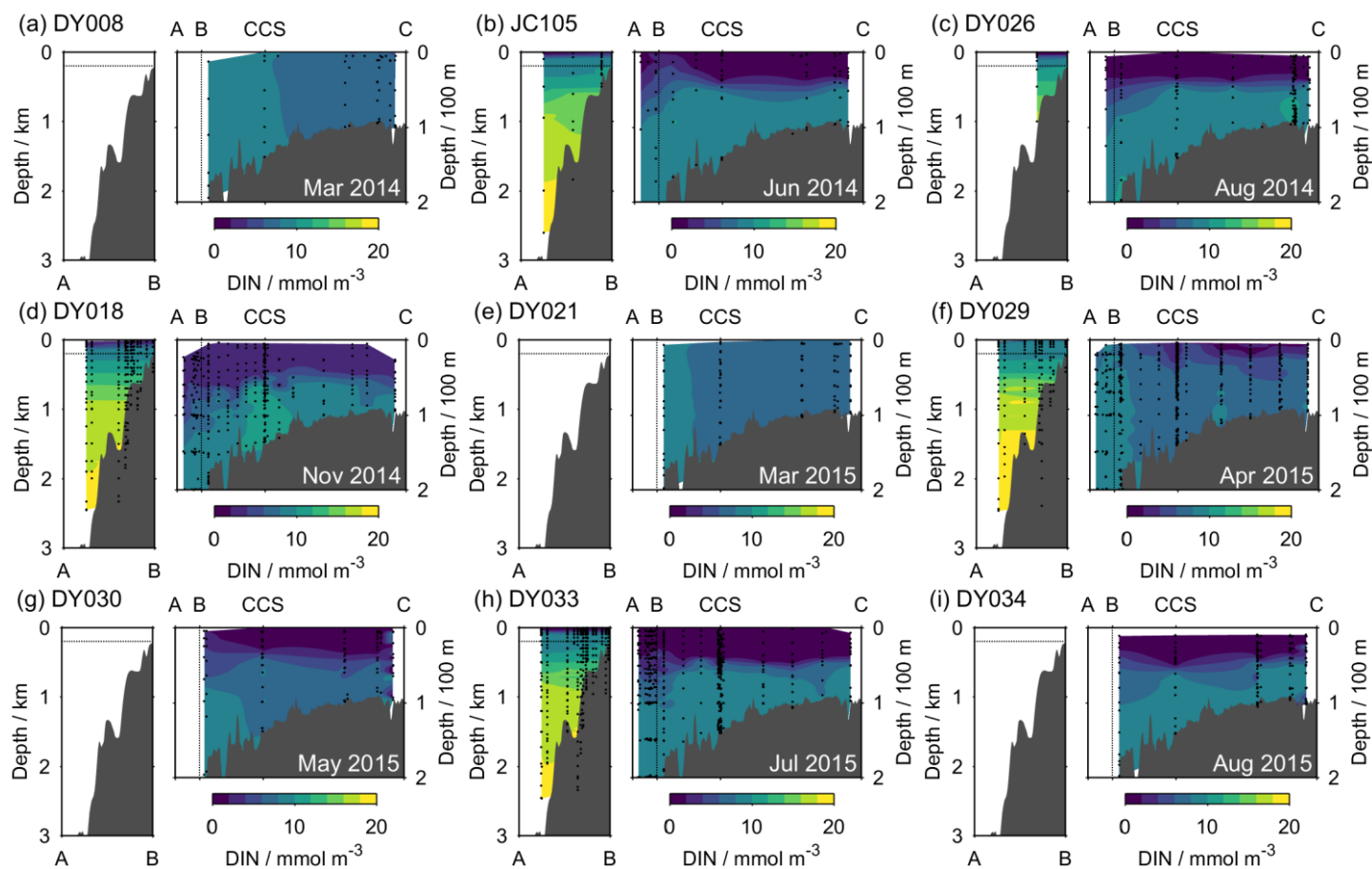


Figure S9. Transects of dissolved inorganic nitrogen (DIN, nitrate + nitrite + ammonium) across the Celtic Sea for all of the UK-SSB cruises. In each panel, the area above the horizontal dotted line in the left plot is the same as that to the left of the vertical dotted line in the right plot. Black circles indicate sample locations.

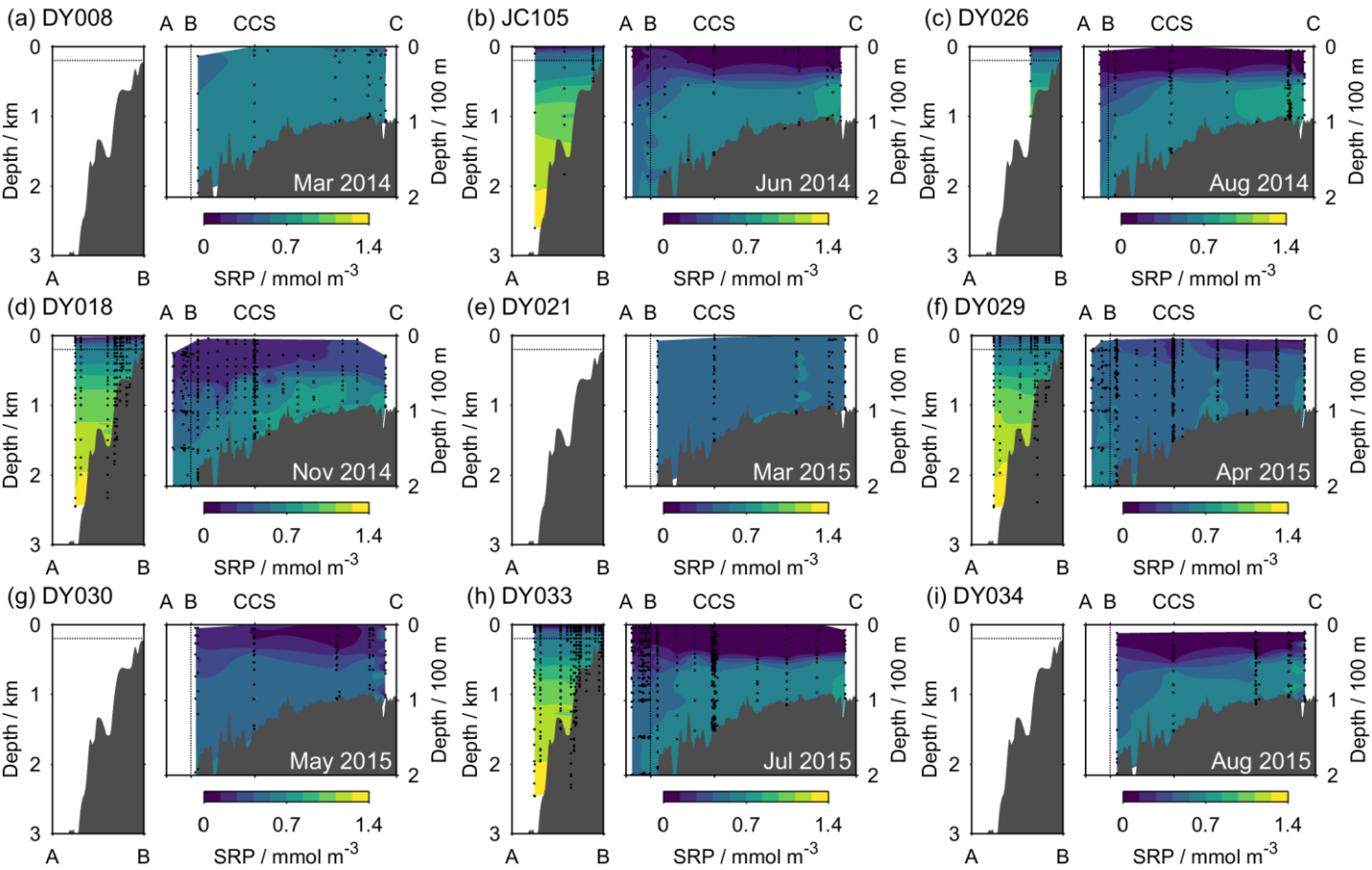
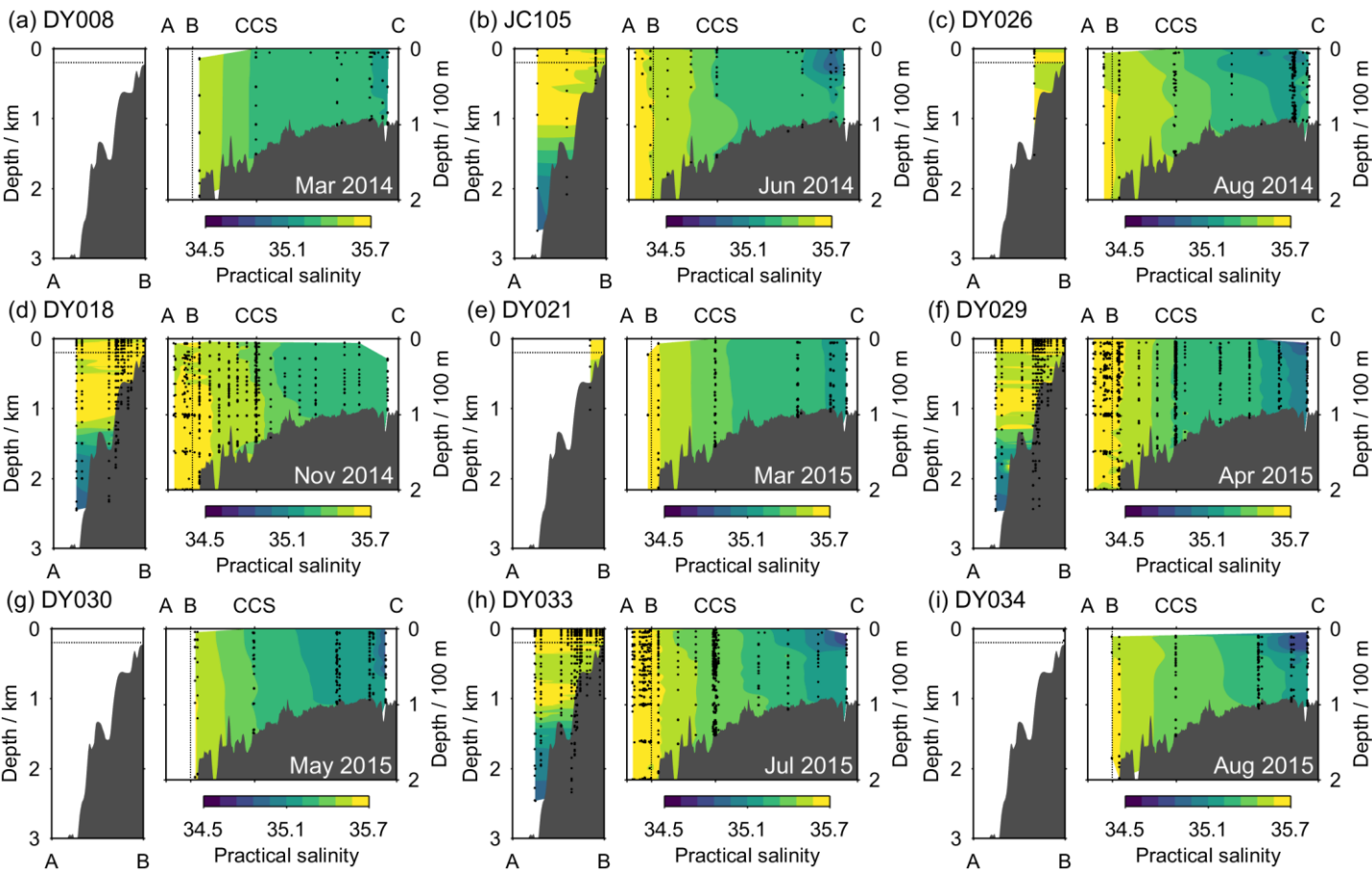


Figure S10. Transects of soluble reactive phosphorus (SRP) across the Celtic Sea for all of the UK-SSB cruises. In each panel, the area above the horizontal dotted line in the left plot is the same as that to the left of the vertical dotted line in the right plot. Black circles indicate sample locations.



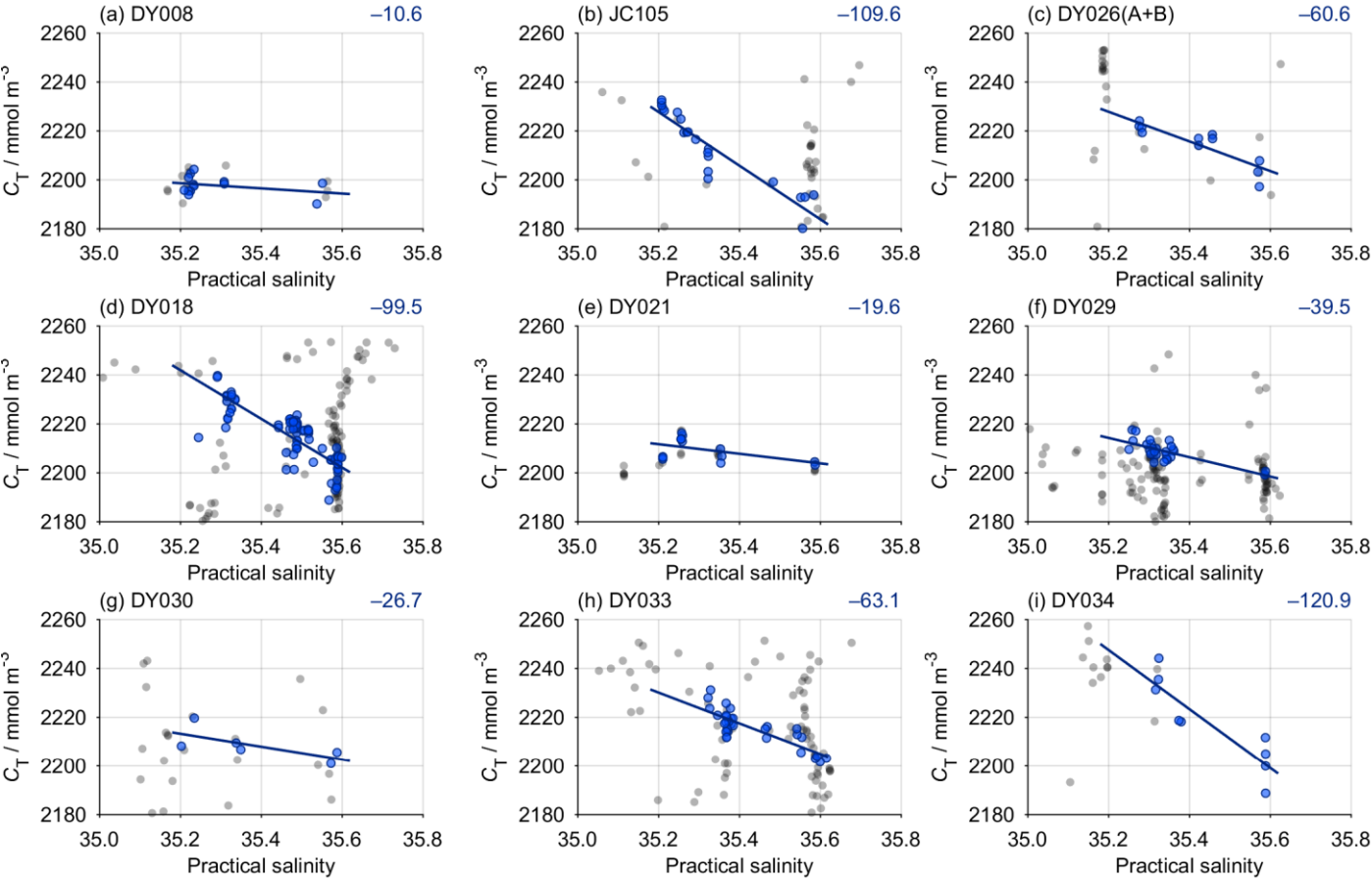
1296 Figure S11. Transects of practical salinity across the Celtic Sea for all of the UK-SSB cruises.
1297 In each panel, the area above the horizontal dotted line in the left plot is the same as that to
1298 the left of the vertical dotted line in the right plot. Black circles indicate sample locations.

1299

1300

1301

1302



1314 Figure S12. Relationship between dissolved inorganic carbon (C_T) and practical salinity for
1315 each UK-SSB cruise. The points used to generate each regression are shown in blue (Section
1316 2.8), and the slope is indicated towards the top right of each panel (see also Fig. 7 and Table
1317 3).

1318

1319

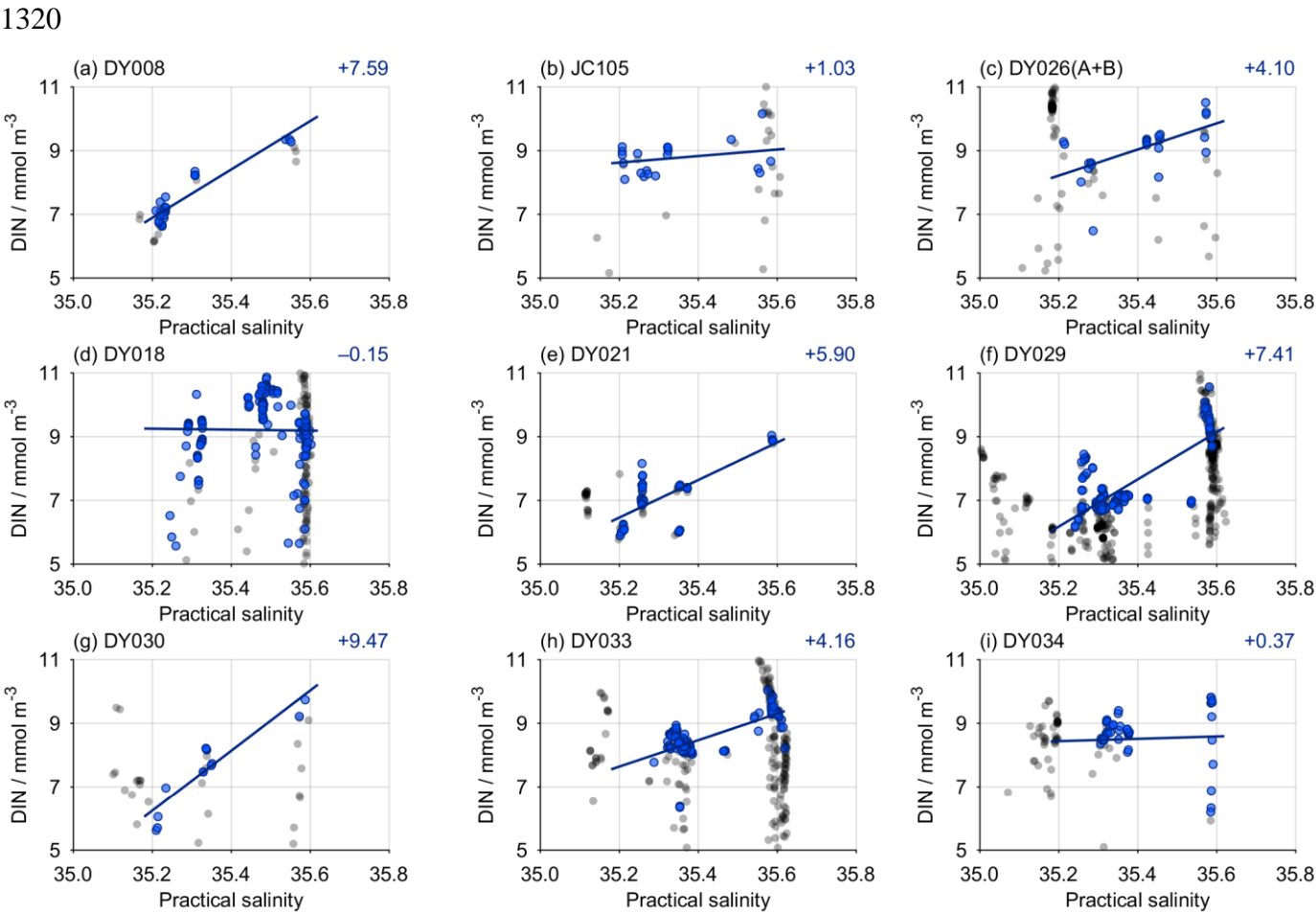
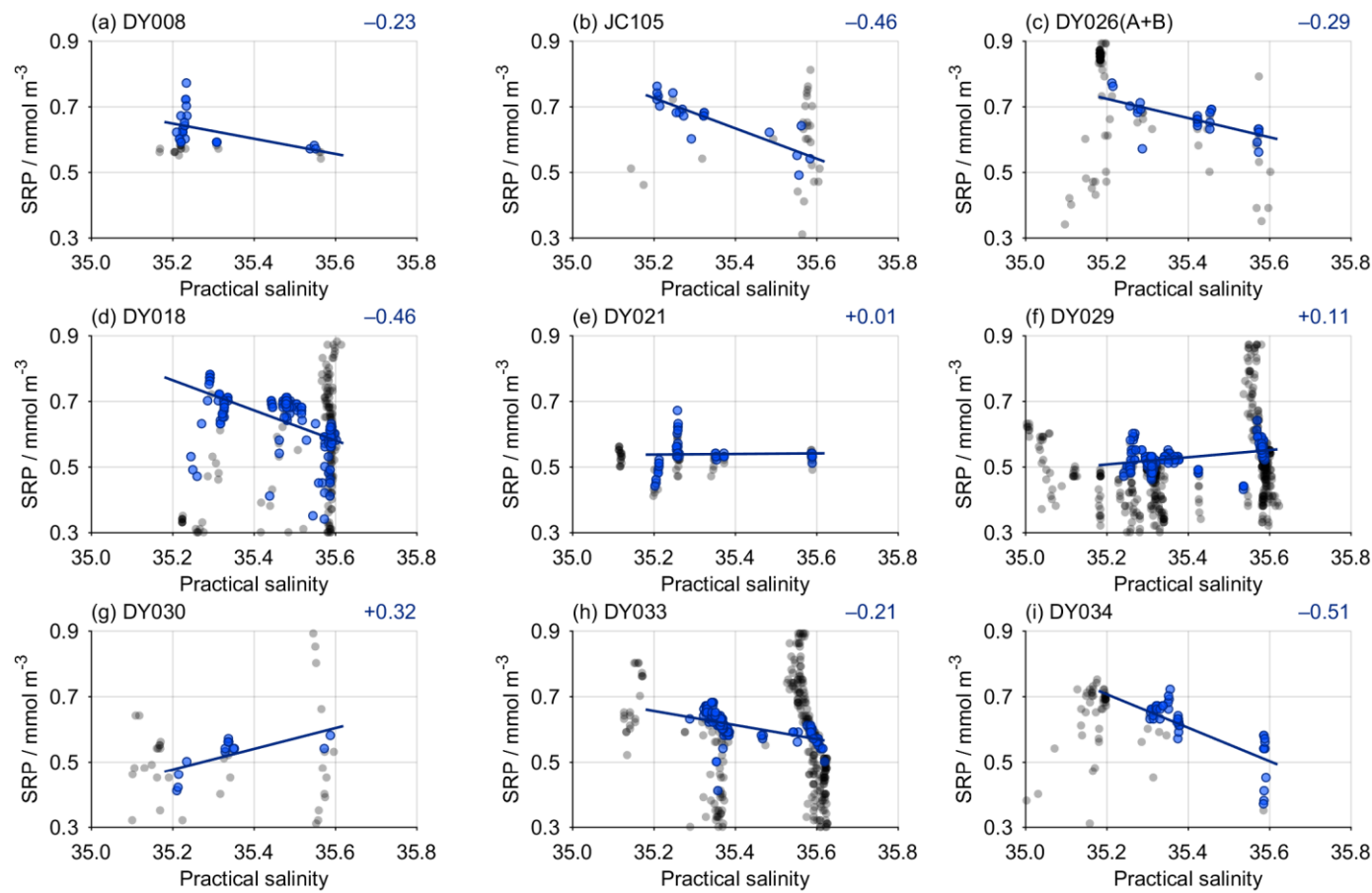


Figure S13. Relationship between dissolved inorganic nitrogen (DIN, nitrate + nitrite + ammonium) and practical salinity for each UK-SSB cruise. The points used to generate each regression are shown in blue (Section 2.8), and the slope is indicated towards the top right of each panel (see also Fig. 7 and Table 3).

1337



1349 Figure S14. Relationship between soluble reactive phosphorus (SRP) and practical salinity
1350 for each UK-SSB cruise. The points used to generate each regression are shown in blue
1351 (Section 2.8), and the slope is indicated towards the top right of each panel (see also Fig. 7
1352 and Table 3).

1353